Determining convective precipitation using cold cloud top temperatures and it's impact on aviation industry over western part of Kenya.

By

DAVID KOROS

I56/79890/2012

Department of Meteorology,

University of Nairobi,

Box 30197-00100,

Nairobi,

Kenya.

A dissertation submitted in partial fulfillment of the requirements for the award of the degree of Master of Science in Aviation Meteorology, University of Nairobi,

Kenya.

May, 2014.

Declaration

This dissertation is my original work and has never been presented for examination in this University or elsewhere.

Signature: Date

---------- ----------

David koros
Department of Meteorology
University of Nairobi

This dissertation has been submitted for examination with our approval as University Supervisors

Signature: Date

---------- ----------

Prof. Joseph M. Ininda
Department of Meteorology
University of Nairobi

Signature: Date

---------- ----------

Dr. Raphael E.A. Okoola
Department of Meteorology,
University of Nairobi

Dedication

I dedicate this study to my wife Christine, My daughter Laurine and my sons Ian and Ryan for inspiring me to work on convections which is a common weather phenomenon in my home area of Kericho and their support throughout the study period.

Abstract

This study quantifies satellite infrared 10.8 μm band cold cloud top temperature data with convective rainfall by matching the cold cloud top temperature threshold values less than 255^0K (-18^0C) of the same spatial and temporal pixel domains with the convective rainfall events from ten synoptic stations. The period of study was for five years from January 2008 to December 2012 over western part of Kenya characterized by rapid variations of convective features which are difficult to detect in the absence of meteorological tracking and detection systems.

Diagnostic techniques of using the derived satellite cold cloud top temperatures threshold values were investigated using statistical methods to assess the predictability potential with the aim of determining strength of indices associated with convective rainfall events.

Significant negative correlations were observed between the convective rainfall and the cold cloud top temperature indices with the highest skill scores obtained during March, April and May long rainy season and October, November and December short rain season. Weak signals were observed during January, February, June, July, August and September.

The results indicated that most convective rainfall events from all the zones occurred for cloud tops temperatures between 235^0K (-38^0C) and 255^0K (-18^0C) with the highest probability of detection at 90% over western zone during the month of April while all the zones recorded over 60% during the same month.

The observed probability may be linked to Intertropical convergence zone (ITCZ) migratory characteristics over the region which reflects the intensity of the convective systems during the months of March to May. Correlation coefficient magnitude was highest at -0.8 indicating that as the cloud top temperature decreases the deep convective clouds extending to high altitude became more active signaling the possibility of more precipitable water over the region.

This suggests that satellite information can be used during short and long rainy seasons as a proxy for convective rainfall. Thus satellite infrared information is useful in convective short range weather predictions notably in mitigation strategies of reducing the effects of adverse weather associated with icing, thunderstorms and downdrafts that are dangerous to aviation in the region.

Acknowledgements

This research was supported by University of Nairobi, Department of Meteorology and Kenya Meteorological Services especially Business Support Service, Data Management Division, Numerical Weather Prediction (NWP) and Severe weather forecasting section.

I thank my colleagues for their assistance during the entire period of my study. Special thanks to Prof. J. M. Ininda, Dr. R. Okoola of the University of Nairobi who supervised me throughout my research work, staff of Department of Meteorology from UoN headed by Dr A.O.Opere and also Dr. J. R. Mukabana, Director of Kenya Meteorological Services.

Lastly I appreciate any contribution to this project work from any other person. May God bless all. Thank you.

Table of Contents **Pages**

List of Figures **Pages**

List of Tables **Pages**

Acronyms and Abbreviations

C	Centigrade
CC	Correlation coefficient
CCTT	Cold Cloud Top Temperatures
C_L	Lift coefficient
COSMO	Consortium for Small Scale Modeling
DCP	Data Collection Platforms
C_D	Total drag coefficient
DWD	Detlev Majewski of Deutsche Wetterdienst
e	Air density
EM	Electromagnetic waves
ENSO	El Niño Southern Oscillation
EUMETSAT	European Meteorological Satellite
F_D	Total drag force
Hpa	Hectopascals(Millibars)
IR	Infrared
ITCZ	Inter Tropical Convergence Zone
JF	January-February
JJAS	June- July -August -September
K	Kelvin
KM	Kilometre
KMS	Kenya Meteorological Services
m	Number of stations used

MAM	March -April -May
MCS	Mesoscale Convective Systems
MJO	Madden-Julien Oscillation
MSG	Meteorological Second Generation
n	Sample size
N_i	Monthly precipitation of the surrounding stations
N_x	Monthly precipitation of the station
OT	Outside Temperature
OND	October -November -December
POD	Probability of Detection
PPT	Precipitation
P_i	Rainfall for station used
P_x	Station rainfall estimate
QBO	Quasi Biennial Oscillation
r	Pearson correlation coefficient
RPM	Revolution per minute
S	Wing surface area
SEVIRI	Spinning Enhanced Visible and Infrared Imager
SST	Sea Surface Temperatures
V	Velocity
ω	Rainfall Value
WMO	World Meteorological Organization

CHAPTER ONE

1.0 INTRODUCTION

Convective weather is known to be associated with hazardous phenomena which include heavy precipitation accompanied by thunderstorms, hailstorms, icing, severe wind gusts, and downbursts, turbulence, lightning or even tornadoes which adversely affect aviation industry.

Convection play a vital role in the vertical transport of heat, moisture, mass, momentum and vorticity from the lower to upper troposphere produced by differences in buoyancy arising from variations in density in an unstable atmosphere (Asnani 2005). Convection occurs in the presence of moderate low level shear that is associated with the southwesterly monsoonal flow and midlevel easterly jets.

While the planetary and synoptic systems provide the trigger mechanisms for active convections during the rainy seasons of March, April and May (MAM) and October to December (OND). Much of the rainfall during these seasons is associated with convective cells.

The rainfall pattern of the regions is bimodal as a consequence of the longitudinal migration of the Inter Tropical Convergence Zone (ITCZ), which is the main rainfall generating system caused by convergence between the southeasterly and northeasterly monsoons that are generated by the sub tropical anticyclones both in the northern hemisphere (Azores and Arabian) and southern hemisphere (St Helena and Mascarene).
Analysis and forecasting of convective weather are thus of the utmost interest for prevention and mitigation against the associated aviation hazards.

Satellite information constitutes an alternative way of studying convective atmospheric cells development which are sudden, deformable and short lived. Convective cells that evolve very fast require high spatial and temporal resolution for precise diagnosis and forecasts. Satellite observations are used to understand the timing, duration and frequency of deep convection (Laing and Carbone, (2011)).

Thus knowledge about the evolution of convective systems is important in improving weather forecast over the tropics.

1.1 Challenges of weather observations in the region

The challenges of weather observations include but not limited to sparse and uneven distribution of gauged rainfall stations, lack of data measurements in remote areas for storm detections, poorly maintained and calibration of instruments.

1.2 Challenges of forecasting convective weather

The rainfall regimes are significantly modified by the mesoscale circulation systems generated by lakes, the high ground areas or mountains, forests/ vegetations, rivers and strong solar insolation that influence diurnal variation of convective systems. These give rise to strong mesoscale circulation within 24hrs period where Lake Breeze dominates the afternoon/evening over the land and land breeze dominates late night/early morning over the lake.

Evolutions of convective storm events associated with hazardous convective weather phenomena pose challenges to short range forecasting. Fast evolving convective atmospheric cells development require high spatial and temporal resolution for precise diagnosis and forecasts.

Thus improvement in analysis and forecasting of convective storms are important strategies necessary for safety of life and property.

In the absence of conventional methods of radar storm detections, sparse, uneven distribution of station networks and lack of data measurements in remote areas and over the ocean, satellite imagery from Meteosat Second Generation Spinning Enhanced Visible and Infrared Imager (MSG-SEVIRI) potentially identifies sudden and short lived convective storms evolving over these regions (Thies et al,2008b).

A convective cell is a cloud with low temperature and composed of two distinct regions, the actual convective part consisting of coldest vertically extended cores and the stratiform region characterized by a more uniform texture and lighter precipitation (Mecikalski and Bedka, 2006). The stratiform area is partly produced by the dissipation of older convective cells and partly produced by broader sloping mesoscale layer ascent. The horizontal patterns formed by the convective core and the stratiform cloud part exhibit large variations and constitute important indicators of the internal cloud dynamics.

The study of the convective precipitation requires high spatial and temporal resolutions for precise diagnosis and forecasts.

The meteorological second generation geostationary space borne sensors provides a wider variety of image channels with narrower bandwidths and an increased spatial and temporal resolution suitable for tracking, detection and analysis of synoptic to mesoscale convective systems necessary for short range forecasts (carbone et al 2002).

While there are various factors responsible for challenges facing aviation industry in the region, the major factor is convective weather related phenomena such as thunderstorms accompanied by heavy rainfall, lightning, hail, strong winds and wind shear that cost the industry economic loss in fuel consumption, inefficiency through delay, cancelation and flights rerouting and event accidents/incidents(Miner et al., 2009) .

On a day to day basis aircrafts are routed to take advantage of the jet stream tailwind to improve fuel efficiency and airports often change runway to increase lift from headwind. These reduce the distance required for takeoff and eliminate potential crosswinds.

Thus there is need to produce and disseminate accurate spatial and temporal aviation weather forecasts that influence the distribution of air services for safe and efficient operations.

This study will focus mainly on the diurnal variation of cold cloud top temperatures (CCTT) and their relationship with the evolution of convective storms over western part of Kenya.

1.3 AREA OF STUDY

The study domain is western part of Kenya which is bounded by longitudes ranging from 34°E to 38°E and latitudes 2°N to 3°S and it is located in the eastern part of African as shown in figure 1 below.

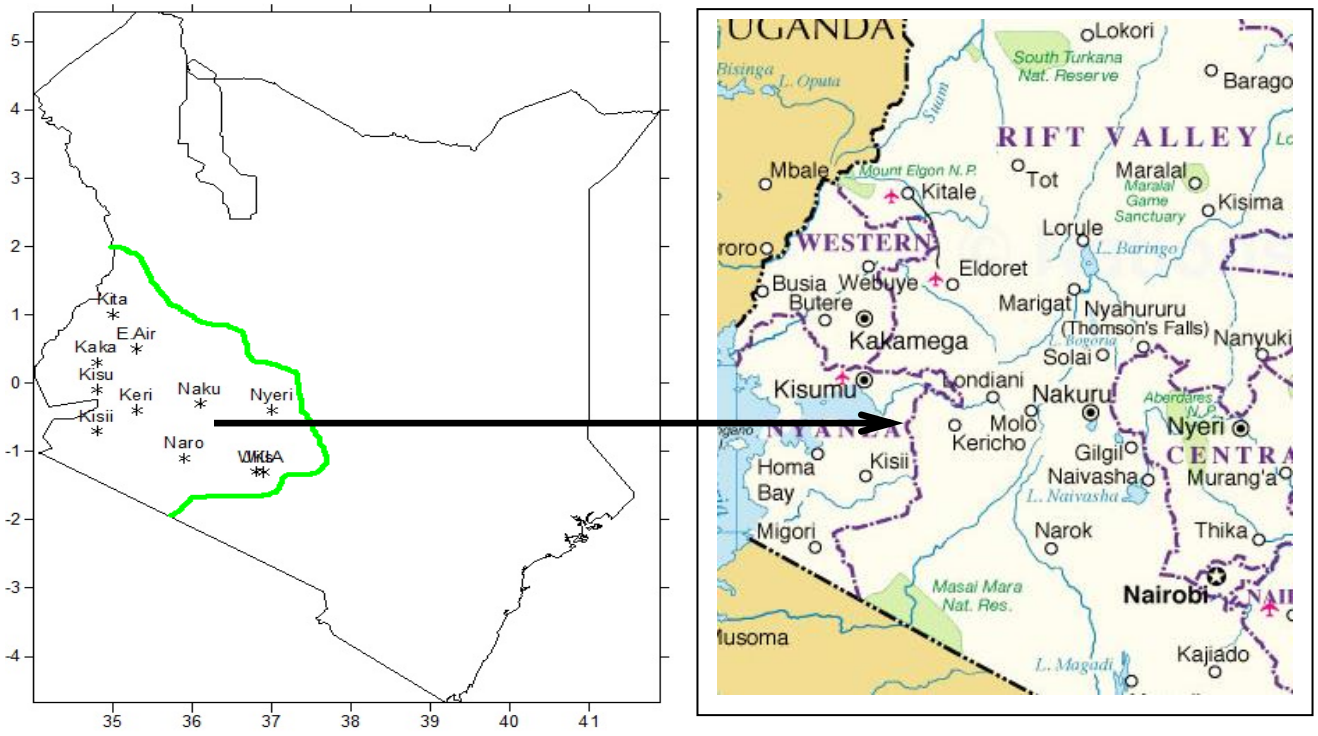

Fig.1: Maps showing the area of study on left and physical features on right panels respectively. Physical features map courtesy of world atlas

1.4 Physical features to east of Lake Victoria Basin

The topography of western parts of Kenya is complex consisting of the highlands and mountain ranges, the Great Rift Valley that runs from north to south, forests, lakes and a network of river systems. Topographical diversity and proximity of Lake Victoria determine the climate characteristics of the western part of the country. Active convections form in this area with heavy precipitation in most afternoons and early mornings (Tomsett, 1994, Asnani, 2005).

1.5 Rainfall climatology of the region

The area is potentially convective unstable, this may be attributed to the availability of the moisture and heating during the rainfall seasons associated with the shifting position of the Inter Tropical Convergence Zone (ITCZ), High pressure cells, monsoons, easterly waves, Tropical cyclones, intra-seasonal waves like the Madden-Julian Oscillations (MJOs) and teleconnections (QBO, ENSO, and western Indian ocean SSTs).

1.5.1 Inter Tropical Convergence Zone (ITCZ)

ITCZ is the main rainfall generating system caused by convergence between the southeasterly and northeasterly monsoons that are generated by the sub tropical anticyclones both in the northern hemisphere (Azores and Arabian) and southern hemisphere (St Helena and Mascarene). The rainfall pattern is bimodal as a consequence of the longitudinal migration over the region.The long rains (March to May) and the short rains (October to December) (Schreck and Semazzi (2004), Indeje *et al*, (2000)). Climate of the region is mainly influenced by the seasonal shift of the ITCZ as well as by mesoscale factors like the complex terrain, contrasts in vegetation types and large inland lakes.

1.5.2 Sea surface temperatures (SSTs) and El Nino Southern Oscillation (ENSO)

Sea surface temperatures (SSTs) have a stronger prediction potential for rainfall over the east African (Mutai *et al*., 1998). The largest rainfall variability during the OND season is mainly associated with SST anomaly forcing of which El Nino Southern Oscillation (ENSO) and Indian Ocean Dipole (IOD) are the dominant sources of inter-annual variability across the region (Ogallo 1988 and Indeje *et al*. 2000; among others).

1.5.3 The quasi-biennial oscillation (QBO)

The quasi-biennial oscillation (QBO) is a quasi-periodic reversal in the zonal winds of the troposphere and stratosphere with an approximate periodicity of 28 months (Indeje *et al*., 2000). The phase of the QBO is defined by the mean zonal winds of the equatorial stratosphere. It was found that above normal rainfall in Eastern Africa has been linked with the westerly phase of the QBO while below normal accumulations are more likely during the easterly phase (Okoola, 1999). Low-level westerlies and upper-level easterlies result in above average rainfall due to enhanced convection and zonal wind shears.

1.5.2. The Madden–Julian Oscillation (MJO)

The Madden–Julian Oscillation (MJO) is the dominant mode of tropical intraseasonal climate variability. Precipitation is significantly modulated by the MJO during both the MAM and OND rainy seasons (pohl and camberlin 2006).

1.6 Effect of mesoscale convective systems (MCSs) on rainfall

The rainfall regimes are significantly modified by the local circulations such as Lake Victoria, mountains and strong solar insolation that causes steep temperature gradients between the water surface and the surrounding high grounds as a result of the overhead sun. These give rise to strong mesoscale circulations over the region. Deep convective systems initiated around 0700z in the morning to 1000z in the afternoon and peak during the late afternoon and evening times around 1200z to 1600z.

The convective systems are westerlies around Lake Victoria tending to easterlies originating from Mau forests then decays towards the morning hours. Lake Breeze dominates the afternoon/evening and land breeze dominates late night/early morning. Meso-scale circulation systems (Indeje *et al*, 2000) control the large spatial and temporal variation in the characteristics of rainfall over the region.

1.7 Large scale systems

The Congo air masses are generally warm and serve to render much of western Kenya generally wet in addition to the lake breeze effect. Low temperatures episodes are common during the Northern summer (June-July-August) due to the effect of cold air advection from the winter south and the warmest period is during the southern summer as dry continental and northeasterly winds flock the region (Mecikalski, *et al*.2006).

The Inter tropical convergence zone (ITCZ) is the main synoptic scale system that controls the intensity and migration of seasonal rainfall over the region. It marks the convergence zone of the atmospheric monsoonal wind system. It is the transitional boundary confluence of the hemispheric winds near the surface as a result of inter-hemispheric monsoon wind systems over the region.

The inter-annual variability of rainfall remarkably throughout most of seasons, the largest portion of this variability is accounted for by the "short rains" season of OND (Mutai *et al*., 1998).

1.8 Other systems affecting weather over the region

Besides ITCZ, the other systems that influence rainfall over the region include sub tropical anticyclones over St Helena, Mascarene, Arabia ridge and Azores regions and their associated ridges.

Other systems affecting the weather over the region are east African monsoonal winds, tropical cyclones, jet streams, and easterly/westerly waves, Equatorial westerly and global teleconnections (QBO, ENSO, MJO and western Indian Ocean SSTs).

1.9 Problem statement

Forecasting of convective storms remains a problem for operational weather forecasting that pose significant threats to safety and economic loss to the aviation industry. Rapid variations of convective weather such as hail, turbulence, lightning and heavy precipitation affect aviation safety and efficiency in the management of both air and terminal operations.

While Numerical weather prediction models provide forecasts on global to regional scales it has low predictive skill for convective precipitation intensity, frequency, timing and location of smaller scales.

The detection of convective features in its early stage still remains a difficult task in the absence of meteorological tracking and detection systems.

Concerted efforts are needed to develop nowcasting convective storm diagnostic techniques with the aim of improving short range aviation weather forecasts that influence the operation of air services.

The use of cold cloud top temperature indices addresses the problem of forecasting trajectory, velocity and intensity of storms through the identification, characteristics, tracking and classification of particular features of convective weather.

1.10 Objectives of the study

The main objective of this study was to quantify significant cold cloud top temperatures that characterize convective rainfalls over western part of Kenya.

The specific objectives are to:-

i. Determine cold cloud top temperature threshold values associated with convective rainfall.

ii. Identify winds circulation patterns associated with active convections.

iii. Assess the predictability of convective precipitation using cloud top temperature indices.

iv. Investigate the economic potential of accurate convective prediction on the operation of airlines.

1.11 Hypothesis

- The satellite data has no bearing on forecasting convective precipitations over western Kenya.
- The satellite cold cloud top temperature indices don't fully characterize the convections.
- The CCTT indices have no predictability potential for thunderstorms.

1.12 Justification of study

The efficient operations of aerodromes require update of the state of the weather and forecast. Convective rainfall occurring at the aerodrome or within it's environ may have devastating impact.

Despite the spatial and temporal resolution of satellite images, convective cloud systems exhibit a complex dynamics in which cells split, merge or change between two successive clouds systems.

The reconstruction of a continuous trajectory to infer the evolution of convective systems in terms of cells development and decay time or active phases constitutes an important aspect in detection and tracking from satellite IR images.

Prediction techniques provide successive estimations of the storm cells location, velocity and trajectories. Hence improvement in predictability of nowcasting evolution of convective weather assist in planning of spatial and temporal distribution of aviation workload and towards disaster mitigation of hazardous convective systems that have devastating impacts on the operation of airlines (Bedka *et al*. 2010).

Convective hazards on en route lead to rerouting and diversions that result in excess operating costs and lost passenger time. Lightning and hailstorms damage can remove aircraft from operations and result in both lost revenues and excess maintenance costs.

Frequent occurrences of these convective storms over the region require quick identifications and sufficient information disseminated to allow decision makers plan mitigation strategies.

There is an increased demand through workshops/seminars and other feedback mechanisms by air operators to produce and disseminate accurate high resolution spatial and lead time of aviation weather forecasts for planning and management of air operations for Kenya to achieve vision 2030 in the transport sector.

Horticultural development and business community are likely to expand requiring faster transport systems. Heavy air traffic is likely to be impacted by bad weather.

Skillful predictions and early warning systems strategies of nowcasting diagnostic techniques of convective precipitation that cost the aviation industry economic loss in lost time, fuel, inefficiency through delay, cancelation and flights rerouting and accidents (Mecikalski *et al*. 2002; Murray, 2002) are necessary for preparedness and mitigation of these disasters.

Therefore accurate aviation forecasts reduce the rates of convective hazard related accidents/incidents in aviation such as delays, diversions or cancellations that increase operating costs.

Concerns have been raised by air operators regarding the accuracy, lead time and spatial coverage of aviation weather forecasts such as route and terminal area forecasts.
The study will address the question of nowcast predictability of convective weather using the cloud tops temperature.
High resolution and short term forecast provide critical information to aviation community for the management of air operations, terminal operations, regulations and suppression of the associated convective hazards through involvement of forecasters in storm detection processes using satellite.

In the absence of ancillary meteorological radar data networks, sparse and uneven distribution of meteorological observatories, satellite imagery potentially identifies hazardous storms by evaluating indicators of hazardous storms in infrared data from the Meteosat 9 satellites.
Several algorithms exists using IR data from geostationary satellites, passive microwave data from polar orbiting satellites or a combination. Hence the standard mode of MSG 9 operations is full disk imagery in 12 spectral channels every 15 minutes in Spinning Enhanced Visible and Infrared Imager (SEVIRI) offer solutions.

Therefore a skilful prediction of convective systems would significantly contribute positively to the socio-economic activities particularly at Kisumu and Eldoret international airports, Maasai Mara, Kakamega, Kitale, Kericho and other airstrips in the region.

CHAPTER TWO

2.0 Literature Review

This chapter reviews in detail literature relevant to the study and threshold values which have been developed to characterize convective storms. Infrared cloud top temperature measurements from space are based on the interpretation of the electromagnetic (EM) radiation that is scattered or emitted from clouds, precipitation and underlying surface monitored by the satellite instruments at discrete spectral regions.

Active convection is difficult to predict because of the highly nonlinear dynamic processes occurring on short time scales (minutes to one hour) and lack of observations of moisture and flow kinematics on mesoscale that lead to upward mass transports of water vapor and temperature structures above the convective boundary layer (Mueller *et al*. 1993; Medlin and Croft 1998).

Given the passive detection methods of meteorological satellites, considerable effort must be placed on discerning convection and isolating the signals of active convections due to their microphysical composition of small, supercooled water droplets/ice crystals and high optical depth.

Despite overlapping clouds, effects of gaseous (water vapor and carbon dioxide) and aerosol absorption on IR temperatures, surface reflectance and emissivity and the poor correlation between clouds and ground based radar, the cloud top temperature of storms has been measured using infrared brightness temperature for decades. This allows for the detection of changes in the temperature of clouds and that of the surface during the day and at night. Clouds are usually colder than the surface (land or water). The temperature of the clouds also indicates how tall they are since temperature is inversely proportional to height in the atmosphere.

In the absence of clouds, the satellite measures the temperature of the surface, which could be land or ocean. In the infrared image, warm temperatures are dark and cold temperatures are lighter. In the image, arid regions are hot and therefore dark, while regions at higher latitudes are usually cooler and brighter. Satellite observations have increased understanding of mesoscale episodic convection and precipitation (Carbone *et al*. 2002).

Several attempts have been proposed for an automatic detection and tracking from satellite image data based on temperature threshold of IR images (Kidder, *et al*, 2005).

Despite some notable advances, such as using specific patterns of cloud top temperature to diagnose severe storms (Heymsfield *et al*. 1983; Adler *et al*. 1985), the vertical mass flux in severe thunderstorm causes large divergence at medium level in the outflow (anvil) region related to the areal growth rate of anvil.

$$\frac{1}{A}\frac{dA}{dt} = \nabla.V, \quad \ldots\ldots(1)$$

Where A is the convective system area, V is the horizontal wind vector detectable by satellite imagery. (Heymsfield and Fulton 1988; Adler *et al*. 1991; Heymsfield *et al*. 1991; Spencer et al. 1994; Negri *et al*. 1994; Mohr and Zipser 1996a, b; Okoola *et al*.1996, 2003,) found out that convections tend to form in areas detectable with infrared satellite imagery data. Low cloud top temperatures are associated with deep convections.

As the cloud top temperatures get colder means greater the vertical height extending into the atmosphere that uplift warm, moist and unstable air forming stronger thunderstorms (Platnick *et al*. 2003). When cloud top temperatures warm up it means that the cloud tops are lower than they were before, indicating that the storm is weakening (Thies *et al*. 2008a). Meteosat Second Generation (MSG) was designed to serve the needs of nowcasting applications and numerical weather prediction. The MSG satellites are 3.2 m in diameter and 2.4 m high and spin anti-clockwise at 100 RPM at an altitude of 36,000 km. It provides the imagery coverage every 15 minutes and provides a service relaying data from Data Collection Platforms (DCP), such as buoys. Data from the MSG Spinning Enhanced Visible and Infrared Imager (SEVIRI) instrument aboard the Meteosat-8 and -9 satellites are used as a proxy for convective precipitation.

2.1 Effect of convective weather on the aviation industry

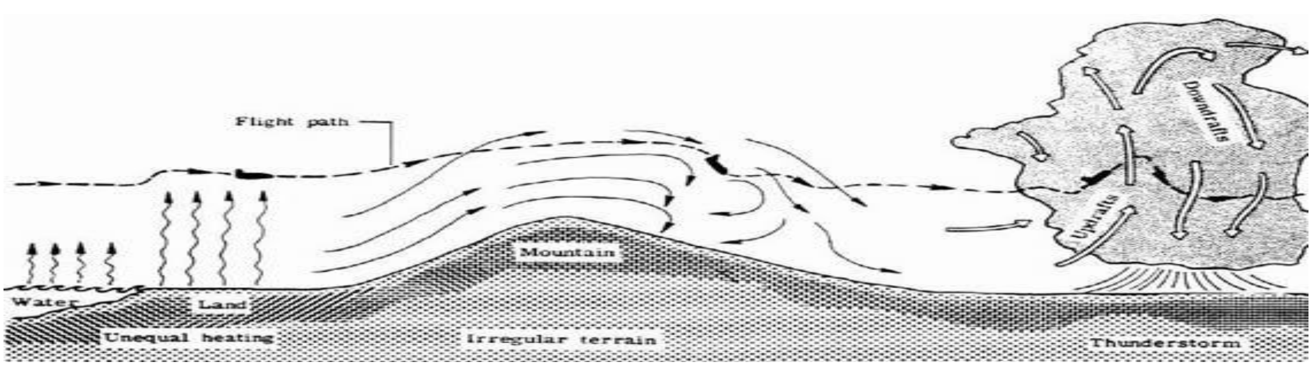

Fig. 2: Effect of hazardous convections on in-flight phases of an aircraft (Murray, 2002).

2.1.1 Take-off/landing convective hazards

Hazardous weather elements on the takeoff and landing phases of flight include turbulence, wind shear and reduced vertical visibility due to clouds. Horizontal hazards may be experienced from rainfall, damaging hail and water ingestion (Sasse and Hauf, 2003). Abrupt changes in wind speed present hazards during take-off and landing which may cause the aircraft to overshoot the runway during landing. Violent thunderstorms draw air into cloud bases with great intensity forming a concentrated vortex from the surface of the ground leading to adverse yaw. Microburst produces strong surface winds which destabilizes an aircraft taking off or landing. Rapid changes in atmospheric pressure during takeoff affect lift force generated by an aircraft given by the equation below.

$$L = C_L \times \tfrac{1}{2} e v^2 \times S \quad \text{.....(2)}$$

Where L is lift equal to plane weight, C_L is lift coefficient, S is wing surface area, e is air density, v is the velocity of aircraft and $\tfrac{1}{2} e v^2$ is dynamic pressure.

2.1.2 Deep convective hazardous weather on cruising stages

Deep convective clouds with great vertical extent in the atmosphere characterized by turbulent, gusty winds and hail or Ice affect performance of the aircraft on cruising stages.

Gusty winds stalls aircraft flying at rough air speed or cruising speed by affecting dynamic lift and drag forces.

$$F_D = C_D \tfrac{1}{2} e v^2 \times S \quad \text{.....(3)}$$

Where F_D is the total drag force, C_D is drag coefficient, S is wing surface area and $\tfrac{1}{2} e v^2$ is dynamic pressure.

Deep convective clouds reduce vertical visibility and heavy precipitation and water ingestion reduce horizontal visibility (Bedard, 2003).

2.1.3 Lightning

Static electricity build up in the airframe when an aircraft enter heavily charged convective cloud directly interfere with the communication systems. Lightning disrupt electric circuit causing structural damage and may ignite the fuel vapor in the fuel cells and distort aircraft parts (Uman & Rakov, (2003); Larsson, 2002).

Lightning indirectly damage avionics systems while sounds and light causes hearing, blindness other physiological problems to passengers and pilot if visual instruments are in use (Petrov & Waters, 1994, 1995).

2.1.4 Heavy precipitation

The thunderstorm contains vast amounts of liquid water droplets suspended or carried aloft by the updrafts. The heavy rain showers encountered during approach and landing reduce visibility and cause retraction on the windscreen of the aircraft and may lead to overshooting the runway during landing. Flooded runway may cause hydroplaning which destroys the braking action needed to bring the aircraft to a stop within the confines of the airport runway and may lead to loss of control during take-off.

Wet runway reduces stopping ability upon landing and decrease steering control on flooded airfields (Wan *et al*, 2009).

2.1.5 Aircraft icing

Ice accretion on the airframe modify the airflow pattern around airfoil surfaces such as wings and propeller blades leading to loss of lift, increased drag and a shift in the airfoil center of pressure. Longitudinal stability may be affected by a degradation of lift generated by the horizontal stabiliser. The ice accretion modify airflow pattern that alter the pressure distribution around flight control surfaces such as ailerons and elevators causing uncontrolled deflections by the pilot. Blockage of the air inlet to any part of a pitot static system produces errors in pressure instruments such as altimeters, airspeed indicators and vertical Speed indicators. Ice forming on unheated aerials can degrade the performance of communication systems (Politovich, 1993).

2.1.6 Hazardous convective weather to aircraft on the ground

The hazardous weather elements such as accumulating hailstones on the ground may lead to aircraft overshooting the runway during landing. Heavy precipitation accompanied by strong surface winds and hailstones inflicts serious mechanical damages to aircrafts on the apron, hangers and parking on open airfields (Bedard, 2003)

CHAPTER THREE

3.0 Data and Methodology

This section discusses the data and the methods that were used to achieve the objectives of the study.

3.1.1 Sources of data

The data used in this study comprised of daily rainfall and associated convective phenomena from ten synoptic stations from the area of study which consisted of Kisumu and Kisii representing the lake basin zone. Western zone was made up of Kakamega, Eldoret Airport and Kitale stations while Kericho, Nakuru and Narok represented Central Rift valley Zone and lastly Nairobi area zone included Jomo Kenyatta and Wilson airports synoptic stations. Observations were taken daily every hour for 24 hours and accumulated rainfalls were recorded everyday at 0600Z (*WMO* standard) from January 2008 to December 2012.

Daily archived coldest cloud tops temperature data with spatial resolution of 3km pixel sampling distance from the same temporal and spatial resolution was extracted from Eumetsat website from http://www.eumetsat.int/Home/Main/DataAccess/EUMETSAT Data Centre from January 2008 to December 2012.

Daily rainfall, wind and other associated convective phenomena data were provided by Kenya Meteorological Services.

Cloud top temperatures data was acquired from European Meteorological Satellite centre (Eumetsat) based in Darmstadt Germany.

Kenya Civil Aviation Authority provided the operational flight data due to adverse convective precipitation.

3.1.2 Data quality control

3.1.2.1 Estimation of missing data

Representative stations with missing rainfall data were filled using cross station correlation matrix where a station with missing record was correlated with all the other stations with complete records and the station that correlates highly with the station in question used to fill the record.

$$P_X = \frac{1}{m}\sum_{i=1}^{m}\left[\frac{N_X}{N_i}\right]p_i \quad \text{----------(4)}$$

Where P_x is estimate for station, P_i rainfall values of station used for estimation, N_x is normal monthly precipitation of the station, N_i is monthly precipitation of surrounding stations and m is number of stations

3.1.2.2 Consistency

The consistency of the data was checked by single mass curve technique to ensure that it was realistic and true representative of the regions. The corresponding cloud top temperatures were subjected to simple quality control procedures to remove possible erroneous reports using mass curves. Inhomogeneity may arise from observation time, method of observation, change in type of instruments, change of site, urbanization, or any other anthropogenic activities. A restriction exists that requires that not more than 10% of missing records should be estimated. Any station that has more than 10% of missing records was discarded from the analysis.

The source station must have a rainfall value (ω) at that point on the time series and the equation estimating the missing value takes the form;

$$\omega_{target} = \frac{\bar{\omega}_{target}}{\bar{\omega}_{source}} \times \omega_{source} \quad \text{----------(5)}$$

The over-bar denotes the mean. Its core to highlight that the two pairs of stations must have high value of correlation coefficient otherwise the estimated values would be erroneous.

3.2.0 Methodology

The main objective of the study was to correlate infrared 10.8 μm band cold cloud top temperatures with convective precipitation and subsequently transforming into statistical presentations.

10.8 μm IR data was used as the primary input to the IR texture overshooting top detection algorithm associated with convective weather at the ground.

Daily infrared 10.8 μm cold cloud top temperature data from January 2008 to December 2012 was used to determine the threshold cold temperatures values associated with precipitation.

The gridded winds (*u* and *v*) data extracted from COSMO Model archives for the year 2012 at 700 hPa level which is the ceiling height of most active convective systems was used to describe the convective motion. The domain of interest in this study covered a region from 2°N to 3° S and 34° E to 38° E and the data/imaging spatial resolution is 3km pixel sampling distance.

3.2.1 Determination of cold cloud tops temperature threshold values

To keep only the cold clouds and thick cirrus associated with convective precipitation, the thresholds cold temperatures between $T_1 = -18^0 Centigrade = 255^0 Kelvin$ and $T_2 = -78^0 Centigrade = 195^0 Kelvin$ were used to separate the convective cells and the core from the other clouds as indicated in table 1.

Table 1: Range of threshold values and associated convective systems

Threshold temperature (T) values in degrees Kelvin	Classification of convections
T≥255	Shallow convections
255≥T≥235	Stratified Convections
235≥T≥215	Deep Convective thunderstorms
215≥T≥195	Severe thunderstorms
195≥ T	Extreme severe thunderstorms

The discrimination of convective cells was performed using a temperature threshold on IR data/imagery since they constitute the coldest events observed by satellite (Laing *et al*. 2008).

Some localized clouds are associated to lifetime between 30 minutes and one hour and a weaker convection activity exhibit temperature below the threshold of -18^oC (Centigrade).

The satellite infrared 10.8um cold cloud top temperatures data of a pixel location was spatially and temporally matched with the convective rainfall events from the same geographical coordinate pixel points from January 2008 to December 2012.

The Western, central rift valley and Nairobi area homogeneous zones for study area were done according to climatic conditions of the area based on Principal Component Analysis (Ogallo, 1980; 1988, Basalirwa 1993, Indeje *et al*., 2000) to capture rainfall stations which have similar temporal characteristics.

Table 2: Location of synoptic stations representing the area of study (*KMS*)

Zone	Stations	Longitude	Latitude	Elevation (ft)
Lake Basin	Kisumu	34.45E	00.06S	3781.8
	Kisii	34.47E	00.40S	5600
Western	Kakamega	34.47E	00.17N	7038.9
	Eldoret Airport	35.14E	00.26N	6402
	Kitale	35.00E	01.01N	6187.5
Central Rift Valley	Nakuru	36.06E	00.16S	6273.3
	Kericho	35.21E	00.22S	7207.2
	Narok	35.50E	01.08S	6237
Nairobi area	JKIA	36.55E	01.19S	5359.2
	Wilson	36.49E	01.19S	5540.7

3.2.2 Assessing the predictability of convective precipitation using cloud top temperature indices

The relationship between the derived cold cloud top temperatures with a convective precipitation was done to investigate the predictability potential using statistical methods.

3.2.2.1 Contingency table threshold analysis

The contingency table was used to determine the strength and weakness of CCTT threshold values less than $255^0 K$. It summarizes the outcome of threshold values and observed precipitation into hit, false alarm, missed and correct negative events.

(i) Hit CCTT threshold values not exceeded and rainfall was observed

(ii) False alarm CCTT threshold values not exceeded but no rainfall observed

(iii)Missed event CCTT threshold values exceeded but rainfall observed

(iv)Correct negative event forecast not to occur, and did not occur

Table 3: Contingence Table

Observed rainfall category	***CCTT threshold category***		
	CCTT $\leq 255\ ^0K$: ***Yes***	CCTT $\geq 255\ ^0K$: ***No***	Marginal total
Rain: Yes	Hits	Misses	Observed Yes
Rain: No	False alarm	Correct negatives	Observed No
Marginal total	Yes: Threshold values	No signal	Total

Observed rainfall category	***CCTT threshold category***		
	Yes	***No***	Marginal total
Rain: Yes	a	b	a + b
Rain: No	c	d	c + d
Marginal total	a + c	b+ d	a + b + c + d

Where *a* represent hits, *b* is misses, *c* is false alarm and *d* represent correct negatives

Hit rate = $\frac{a}{(a+c)}$ ……...…….(6)

Hit rate is the fraction of observed events that were correctly diagnosed.

False alarm = $\frac{c}{(a+c)}$ ……(7)

False Alarm Ratio is the fraction of predicted events that were wrongly diagnosed.

A perfect forecast system produce only hits and correct negatives and no misses or false alarms.

3.2.2.2 Probability of Detection

The probability of detection (POD) is a measure of the ability of the forecast program to successfully predict event. The POD is a measure of the forecast accuracy of precipitation events that accounts for hits and misses. The Probability of detection (hit rate) is given by

$$POD = \frac{hits}{hits + misses} \qquad \text{…(8)}$$

This method has been used by many authors, for example Laing *et al.* (2008), to study the relationship between the mesoscale activities and rainfall over equatorial Africa.

3.2.2.3 Pearson Product Moment Correlation Analysis

The Pearson correlation coefficient, *r*: between bivariate data, X_i and Y_i values ($i = 1,\ldots,n$) where $\overline{X}$ and $\overline{Y}$ are the sample means of the X_i and Y_i values, respectively were computed using Excel; Microsoft by using the option “Correlation” under the option “Data Analysis Tools”.

In the equation 8 below, N is the total number of records, R and CCTT are rainfall events and cold cloud top temperature respectively while

$$r = \frac{\frac{1}{N}\sum_{i=1}^{N}(CT_i - \overline{CT})(R_i - \overline{R})}{\sqrt{\frac{1}{N}\sum_{i=1}^{N}(CT_i - \overline{CT})^2}\sqrt{\frac{1}{N}\sum_{i=1}^{N}(R_i - R)^2}} \qquad \text{…(9)}$$

The purpose of correlation analysis was to measure and interpret the strength of relationship between Cold Cloud top temperature (CCTT) and convective precipitation. The signs of the correlation coefficient (ie, positive or negative) defines the direction of the relationship. The magnitude indicates the strength of the correlation. This method has been used by many authors, for example Ogallo (1988) and Ininda (1994), to study the association between the rainfall and other climatic parameters. For $r^2 = 0$, it implies Lack of fit, while $r^2 = 1$ implies perfect fit.

The student t-test technique was used to test for the significance of the correlation coefficient between the two variables.

$$t_{n-2} = r\sqrt{\frac{n-2}{1-r^2}} \quad \text{.....} \quad \text{.....} \quad \text{.....} \quad (10)$$

3.2.2.4 Winds at 700hpa and 500hpa levels

Assimilated COSMO (Consortium for Small Scale Modeling) atmospheric wind fields at pressure level 700 hPa were used to describe the convective motions which indicated trajectories and velocity of the convective cells. The 700 hPa to 500 hPa level winds correspond to FL100 to F180 with an altitude of about 3 km to 5 km above the sea level and is an approximate ceiling height of active convective systems, the altitude most domestic aircraft fly. The ITCZ is however detectable in the wind field near 700hPa (Kiangi *et al* 1981, Mukabana and Pielke, 1996).

3.2.2.5 Cosmo Model description

The COSMO is the numerical weather prediction model, designed for both operational short range numerical weather prediction and other scientific operations initially developed by Detlev Majewski of Deutsche Wetterdienst (DWD), the meteorological office of Germany. The model is a non hydrostatic limited area atmospheric prediction based on a set of equations that describe the evolution of variables such as wind speed, temperature, humidity, pressure and rainfall that define the weather or the state of the atmosphere. The process starts with analyzed data using observations and previous forecast to obtain the best estimate of the current state of the atmosphere. COSMO is run operationally twice a day: 0000 and 1200 GMT and is fully automated from downloading input files using the preginet server to graphics display of outputs with the total processing time of about one and half hours for 78 hour forecast and horizontal resolution grid spacing of 7 km and 14 km.

The key issue is an accurate numerical prediction of weather conditions focusing on prognostic variables of horizontal and vertical wind components.

Figure 3 below is the satellite imagery on infrared 10.8 um channel over Kenya showing deep convective systems with individual and clusters of convective cells.

Deep convective systems are characterized by cold clouds tops appearing white and warm clouds as well as clear skies appearing dark.

The wind vectors indicated the zones of convergence of convective systems over western part of Kenya.

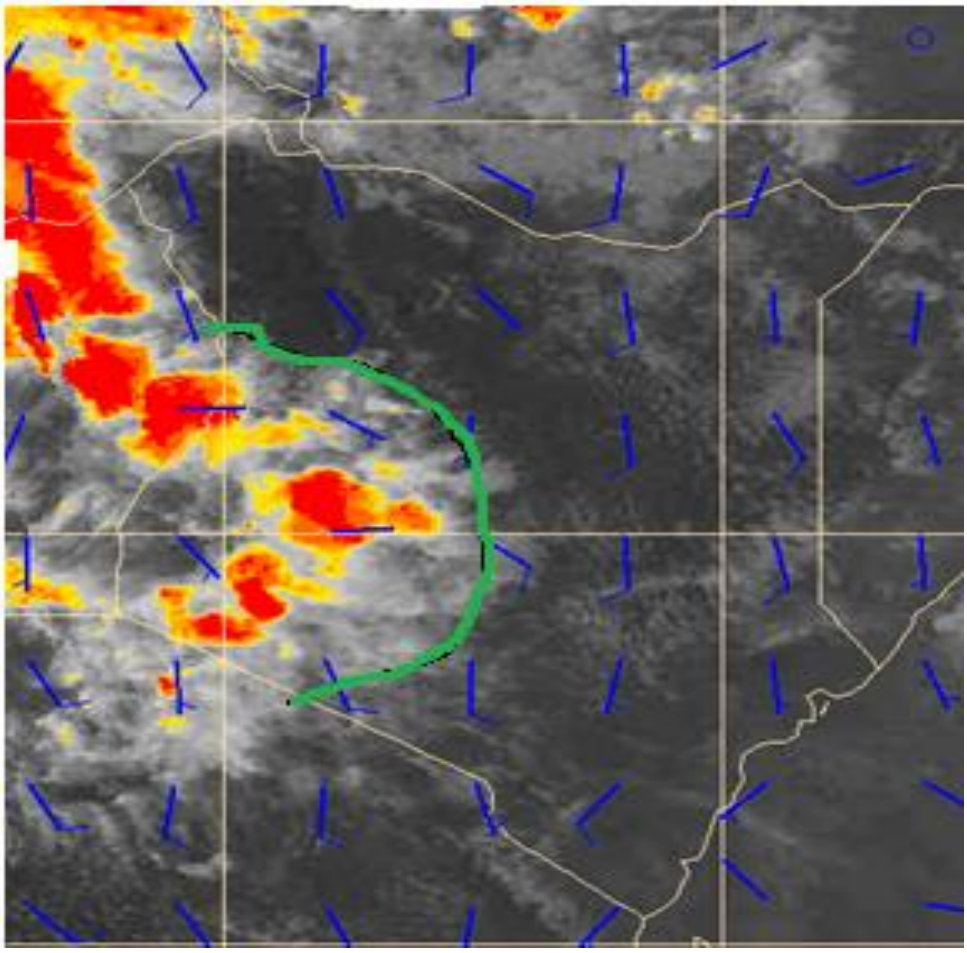

Fig. 3: Medium Level Winds and convective systems from 10.8 IR satellite data on 14th April 2012

3.2.2.6 Assessment of economic impacts of adverse convective precipitation on aviation industry

Simulated data on costs related to adverse weather from previous studies were used in evaluating effect of convective precipitation over western Kenya (Sands *et al*, 2009; Warren, 2009; Muiruri, 2011).

The method was adopted from a report by university of Westminster (2004) where the cost per aircraft delay was estimated at $72 per minute.

The delay arises from adversed convective weather on en-route, departure or destination airport/airstrip of flight that was more than 15 minutes beyond the scheduled departure/arrival times published by the aircraft operators.

Approximate cost of aircraft diversion over the region was assessed using the previous studies (Sands *et al*, 2009; Warren, 2009; Muiruri, 2011) which revealed that the cost ranges between $20,000 to $100,000 depending on the nature of operations, diurnal and seasonal weather characteristics and the size of the aircrafts operating over the western region of Kenya.

The cost included holding of the aircrafts before diverting, the flight time to the diverted airport, the fuel burn, landing fees, ground handling fees, meals to passengers, accommodation, ferrying passengers, as well as lost opportunities by both the aircraft operators and the passengers.

CHAPTER FOUR

4.0 Results and discussion

This chapter presents the results of the study from the methods used to achieve the objectives outlined in section 1.10 of this study.

4.1 Results of cold cloud top temperature (CCTT) threshold values

The results of daily (CCTT) threshold values against daily accumulated averaged convective rainfall data from stations in each zone for the same period were analyzed. Below are the summaries of frequencies in percentages of cold cloud top temperature threshold values associated with convective rainfall events obtained from each zone.

Table 4.1 below indicate the threshold values over the Lake Basin during the period showing the highest mean frequency of 60% of the total convective rainfall events occurred between 235^0K and 255^0K followed by 215^0K to 235^0K with 32%. 8% of the total rainfall events occurred between 195^0K and 215^0K and the lowest frequency was on the threshold values of below 195^0K.

It can be seen from the table that the zone experienced the highest number of active weather at cloud tops temperature of between 235^0K to 255^0K or (-38^0C to -18^0C).

Table 4.1: Frequencies in percentage of CCTT threshold indices over Lake Basin

Temperature (T) in Degrees Kelvin	2008	2009	2010	2011	2012	Mean %
$T^0K \leq 195$	0	0	0	0	1	0
$195 \leq T \leq 215$	7	11	4	8	8	8
$215 \leq T \leq 235$	34	40	33	28	27	32
$235 \leq T \leq 255$	59	50	63	64	64	60

The results of the analysis of threshold values over western zone are shown in table 4.2 below indicating the highest mean frequency of 58% of the total convective rainfall events occurred between 235^0K and $255^0 K$ followed by 215^oK to 235^0K with 33%. 9% of the total convective precipitation events occurred between 195^0K and 215^0K and the lowest frequency was on the threshold values of less than 195^0K.

From the table, it can be noted that a large percentage of convective rainfall occurred at a much colder cloud top temperatures with great vertical height. This explained the strength of the lake breeze that cover large inland areas as compared to land breeze hence deep convective systems are found over the areas away from the Lake basin.

Table 4.2: Western zone frequencies in Percentages

Temperature (T) in Degrees Kelvin	2008	2009	2010	2011	2012	Mean %
$T^0K \leq 195$	0	0	0	0	0	0
$195 \leq T \leq 215$	8	11	4	11	9	9
$215 \leq T \leq 235$	34	39	36	27	31	33
$235 \leq T \leq 255$	58	50	59	63	60	58

From analysis of the threshold values over Central Rift Valley zone during the same period as shown in table 4.3 below, the highest mean frequency of 64% occurred between 235^0K and 255^0K followed by 215^0K to 235^0K with 31%. 5% of the total rainfall events occurred between 195^0K and 215^0K and the lowest frequency was on the threshold values of below 195^0K.

This demonstrated that most active convective weather occur within the threshold values between 235^0K and 255^0K (-38^0 and -18^0C) with substantive occurrence of deep convective clouds with colder tops.

Table 4.3: Central Rift Valley frequencies in percentages

Temperature (T) in Degrees Kelvin	2008	2009	2010	2011	2012	Mean %
$T^0K \leq 195$	0	0	0	0	0	0
$195 \leq T \leq 215$	7	8	5	1	3	5
$215 \leq T \leq 235$	23	30	31	40	32	31
$235 \leq T \leq 255$	70	62	63	59	65	64

Table 4.4 below indicate the distribution of frequencies in percentages of the threshold values over the Nairobi zone showing the highest mean frequency of 67% occurred between 235^0K and 255^0K followed by 215^0K to 235^0K with 32%. 2% of the total rainfall events occurred between 195^0K and 215^0K but no convective precipitation occurred with the threshold values of below 195^0K.

This illustrated the effect of more organized large scales features away from the lake than the complex mesoscales convective systems over the Lake Victoria basin.

Table 4.4: Nairobi area zone CCTT threshold indices frequencies in percentages

Temperature (T) in Degrees Kelvin	2008	2009	2010	2011	2012	Mean %
$T^0K \leq 195$	0	0	0	0	0	0
$195 \leq T \leq 215$	7	2	0	0	0	2
$215 \leq T \leq 235$	37	31	21	35	35	32
$235 \leq T \leq 255$	56	67	79	65	65	67

The distribution of mean frequencies of threshold values over the region are shown in table 4.5 below indicating the highest occurrence of convective precipitation between 235^0K and 255^0K especially from Nairobi zone with 67%. Western zone recorded the highest percentage of precipitation occurring at the coldest temperatures followed by the Lake Basin and central rift valley describing the effect of the proximity of Lake Victoria on the development of mesoscale convective systems.

Table 4.5: Mean frequencies in percentages of CCTT indices associated with rainfall obtained during the period.

CCTT threshold values T in ^0K)	Lake basin (%)	Western zone (%)	Central rift valley (%)	Nairobi area Zone (%)
$T^0K \leq 195$	0	0	0	0
$195 \leq T \leq 215$	8	9	5	2
$215 \leq T \leq 235$	32	33	31	32
$235 \leq T \leq 255$	60	58	64	67

Summary of the frequencies in percentages of CCTT indices associated with convective weather over the region are shown in column chart in figure 4.1.

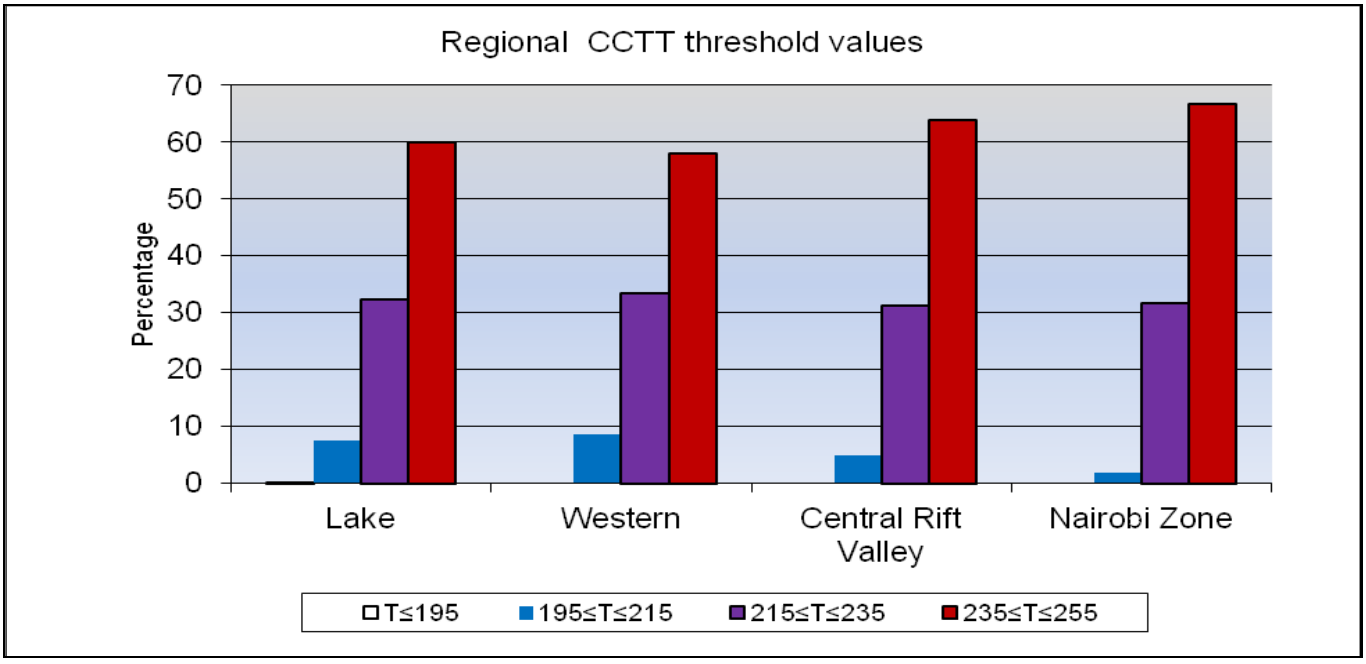

Fig. 4.1: Column chart showing the percentage frequencies of CCTT indices during the period

4.2 Skill scores obtained from each zone of study.

Monthly strength and weakness of CCTT threshold values over the region are summarized in contingence tables below.

Table 4.6 indicate the high number of hits rate over the lake basin during March, April and May long rains and October, November and December short rainy season where the events were correctly diagnosed by the indices with strong signals. Low skill scores were observed during the months of June to September due to advections of cold airmasses over the region from the southern hemisphere characterized by stratified clouds, fogs, drizzles and light rains as shown by high number of misses exhibiting the weaknesses of the threshold values.

The indices registered the highest number of false alarms during January and February dry season as a result of insufficient ingredients for the developments of significant convective precipitation. The CCTT indices captured high signals of no rains during the months of January to February as illustrated by the high number of correct negatives.

Table 4.6: Results from Lake Basin zone indicating monthly scores

Months	**Lake basin**				
	Observed rainfall days	Hits	Misses	False alarms	Correct negatives
Jan	55	28	27	35	65
Feb	70	40	30	27	43
Mar	105	66	39	23	27
Apr	127	86	41	20	8
May	126	66	60	11	18
Jun	106	44	62	6	43
Jul	80	19	61	15	50
Aug	100	23	77	10	45
Sep	130	45	85	7	18
Oct	116	61	55	13	26
Nov	114	70	44	12	29
Dec	109	51	58	8	38

During March, April and May long rains and October, November and December short rainy season over the western zone, the events were correctly diagnosed by the indices with high skill scores as shown by the high number of hits rate in table 4.7 below. Low skill scores were observed during the months of June to September as indicated by high number of misses portraying the weaknesses of the threshold values. High number of false alarms was registered during January and February dry season while the indices captured very well signals of no rains mainly during the months of December to February as illustrated by the high number of correct negatives.

Table 4.7: Western zone monthly skill scores

Months	**Western Zone**				
	Observed rainfall days	Hits	Misses	False alarms	Correct negatives
Jan	45	15	30	36	68
Feb	41	31	20	38	51
Mar	89	69	20	26	40
Apr	117	102	15	18	20
May	135	91	44	9	11
Jun	126	54	72	6	23
Jul	137	47	90	6	12
Aug	141	45	96	4	10
Sep	139	66	73	6	10
Oct	129	72	57	7	19
Nov	96	67	29	25	34
Dec	62	40	22	20	73

High skill scores of CCTT indices were obtained as indicated by the high number of hits rate over the central rift valley zone in table 4.8 below during the months of March to May long rains and October, November and December short rainy season where the events were correctly diagnosed and this coincided with ITCZ over the region. Low skill scores were observed during the months of June to September as indicated by high number of misses. High number of false alarms was registered during January and February dry season. Indices also captured very well signals of no rains during the dry months of January to February as illustrated by the high number of correct negatives.

Table 4.8: Central Rift Valley monthly skill scores

Months	**Central Rift Valley**				
	Observed rainfall days	Hits	Misses	False alarms	Correct negatives
Jan	54	18	46	33	58
Feb	60	28	33	40	38
Mar	88	68	20	32	35
Apr	134	85	49	16	5
May	131	68	63	10	14
Jun	111	33	78	12	32
Jul	124	47	77	7	24
Aug	132	36	96	4	19
Sep	130	42	88	9	16
Oct	136	66	70	13	6
Nov	110	67	43	17	28
Dec	67	36	31	18	70

The skill scores of CCTT indices were high as indicated by the high number of hits rate over Nairobi zone in table 4.9 below during the months of March to May long rains and October, November and December short rainy season where the events were correctly diagnosed and this coincided with ITCZ over the region. Low skill scores were observed during the months of June to September as shown by high number of misses. A high number of false alarms were registered during January and February dry season. Indices also captured very well signals of no rains during the dry months of January to February as demonstrated by the high number of correct negatives.

Table 4.9: Nairobi area zone monthly skill scores

Months	**Nairobi area**				
	Observed rainfall days	Hits	Misses	False alarms	Correct negatives
Jan	19	3	14	28	107
Feb	32	11	21	21	83
Mar	68	51	17	36	51
Apr	107	66	41	17	31
May	101	32	69	19	35
Jun	57	12	45	23	75
Jul	50	10	40	16	89
Aug	66	15	51	16	73
Sep	45	9	36	28	82
Oct	58	31	27	22	75
Nov	100	50	50	21	34
Dec	76	22	54	17	62

4.3 Results of Probability of Detection (POD) using CCTT Indices for the Zones

Probabilities of detection were done for each zone to determine the ability of using the CCTT indices to predict occurrence of convective precipitation.

Table 4.10 below are the results of monthly probability of detection of convective rainfall events obtained over the region indicating the chances of using the indices in predicting precipitation that demonstrated strongest signals over western zone during April long rainy season of 0.9 or 90 percent while the other zones recorded over 60 percent confidence level during the same month. Weak signals as low as 20 percent chances of occurrence of convective precipitation events were observed during the months of June to September.

This shows a mean percent of 75 confidence level of the occurrence of convective precipitation using the CCTT prediction indices during the rainy periods.

Table 4.10: Monthly Probability of Detection of Rainfall Events indicating the confidence level from each Zone

Month	Lake basin	Western	Central rift valley	Nairobi area
Jan	0.5	0.3	0.3	0.2
Feb	0.6	0.8	0.5	0.3
Mar	0.6	0.8	0.8	0.8
Apr	0.7	0.9	0.6	0.6
May	0.5	0.7	0.5	0.3
Jun	0.4	0.4	0.3	0.2
Jul	0.2	0.3	0.4	0.2
Aug	0.2	0.3	0.3	0.2
Sep	0.3	0.5	0.3	0.2
Oct	0.5	0.6	0.5	0.5
Nov	0.6	0.7	0.6	0.5
Dec	0.5	0.6	0.5	0.3

4.4 Time series probability of detection

The aim of the time series was to identify the sequence of the convective rainfall events with respect to CCTT using past events and to predict the trend of the events.

The following trends were obtained during the period as illustrated in figure 4.2 below showing high chances of predictions using the indices during the months of February to May there after reduced to the lowest level between July and September and then started increasing again between October and December before decreasing towards January.

This explained the effect of the longitudinal migration of the Inter Tropical Convergence Zone (ITCZ), which is the main rainfall generating system caused by convergence between the southeasterly and northeasterly monsoons which deepened active convective clouds with cold tops during MAM and OND rainy seasons.

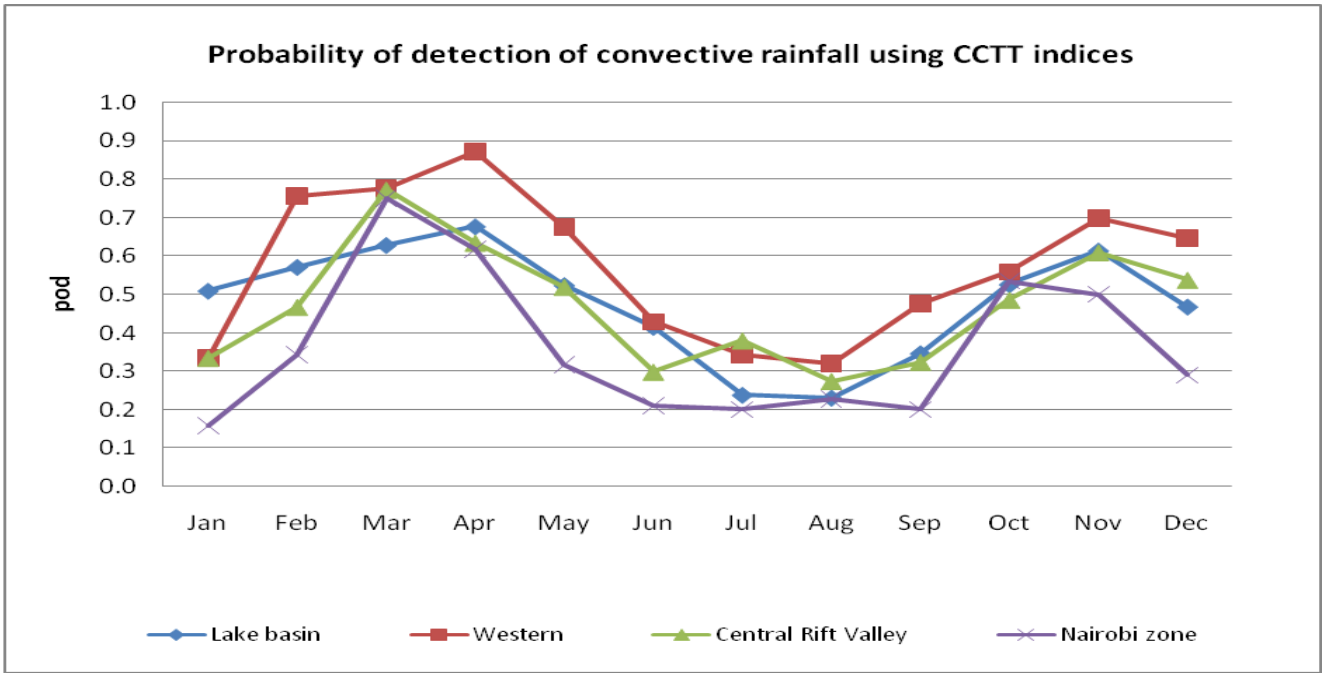

Fig.4.2: Time series monthly probability of detection using the CCTT indices

4.5 Results of Thunderstorms Days and CCTT Values less than 255 ^{0}K associated with severe weather hazardous to aviation during 2011 and 2012.

Figures 4.3, 4.4, 4.5 and 4.6 below indicates monthly trends of thunderstorms days associated with cold cloud top temperatures below 255 ^{0}K (-18^{0}C) which captured positive relationship between occurrence of significant convective systems and the CCTT threshold values especially over the regions adjacent to the Lake Victoria characterized by deep convective systems. This is illustrated in figures 4.3 and 4.5 by high number of thunderstorms days over central rift valley zone around Kericho and Kisii areas in the Lake Basin zone during the months of March to May long rains.

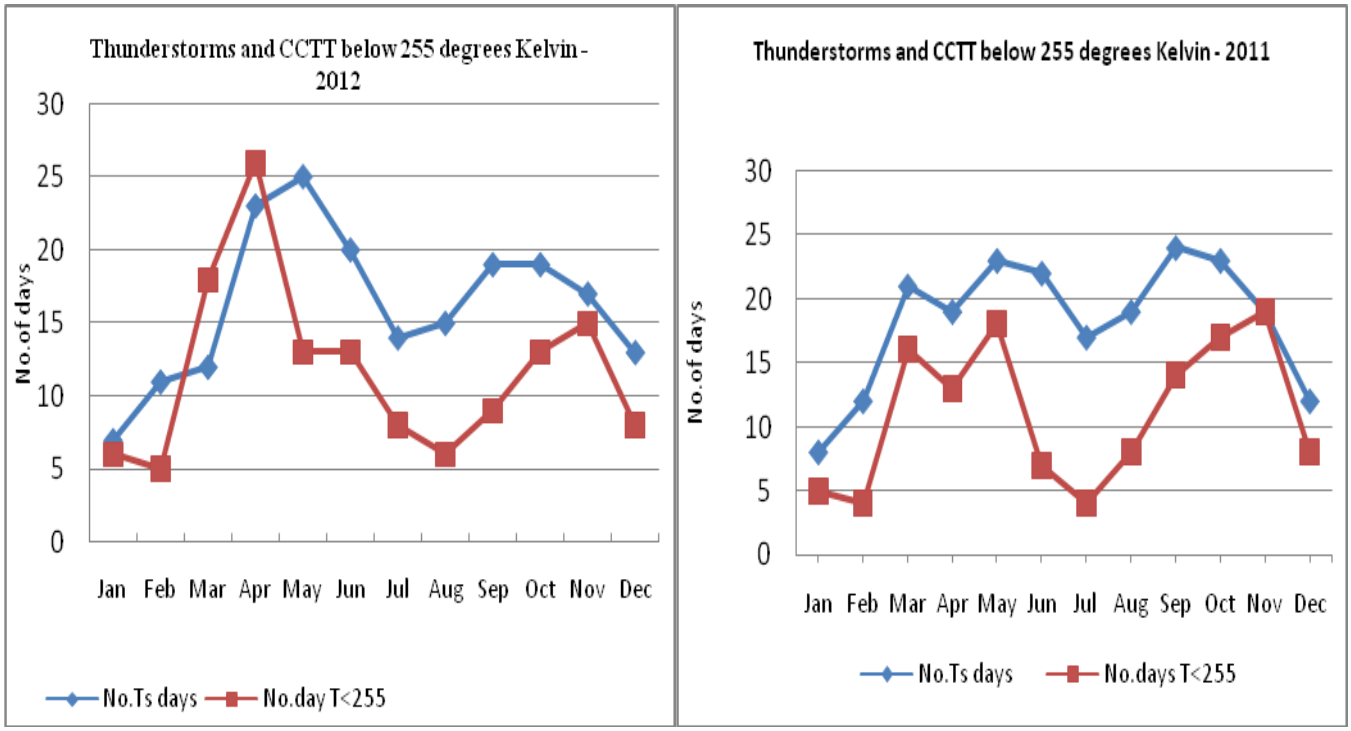

Fig.4.3: Lake Basin zone thunderstorms days associated with cold cloud top temperatures below 255 ^{0}K

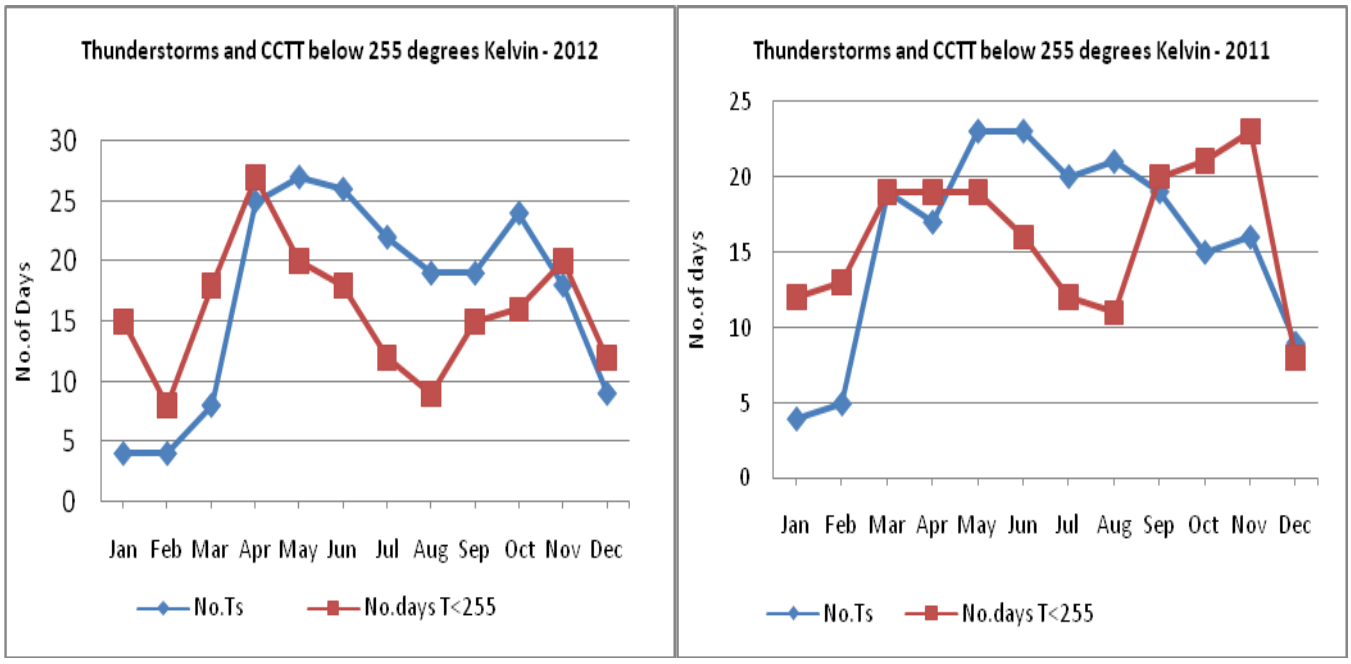

Fig.4.4: Western zone thunderstorms days associated with cold cloud top temperatures below 255 ^{0}K

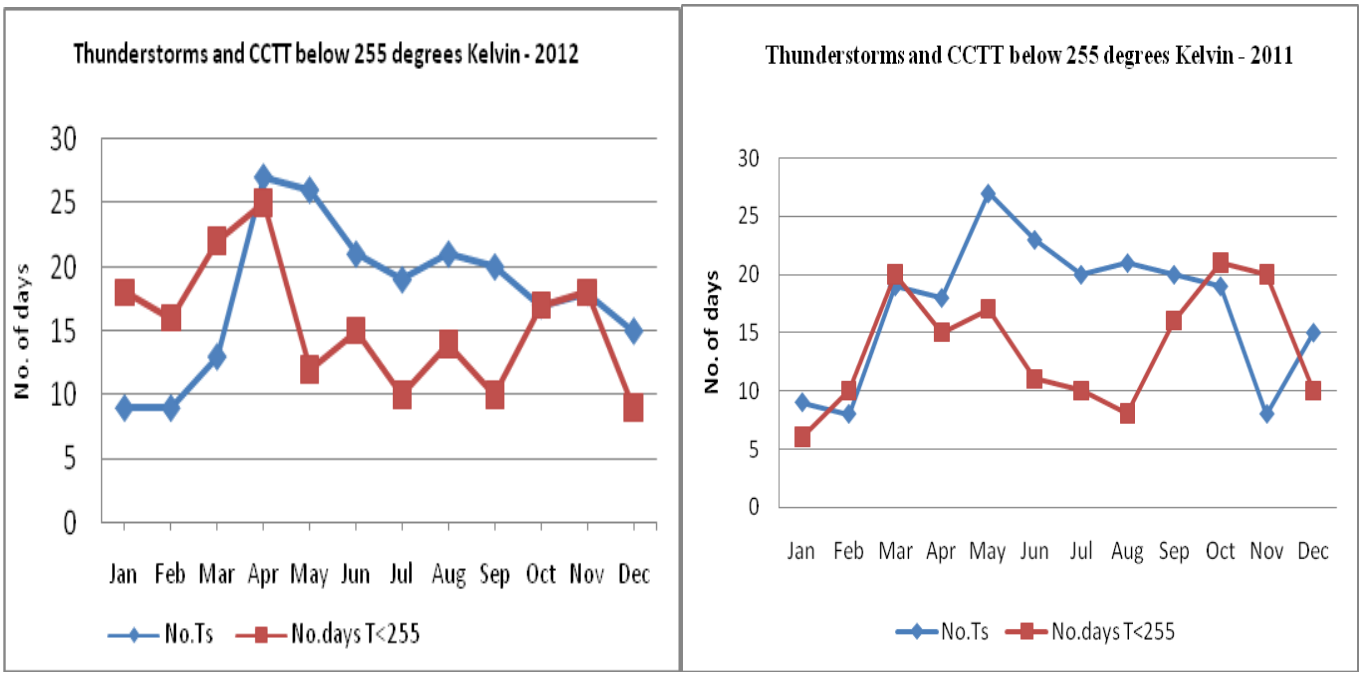

Fig.4.5: Central Rift Valley thunderstorms days associated with cold cloud top temperatures below 255 ${}^{0}K$

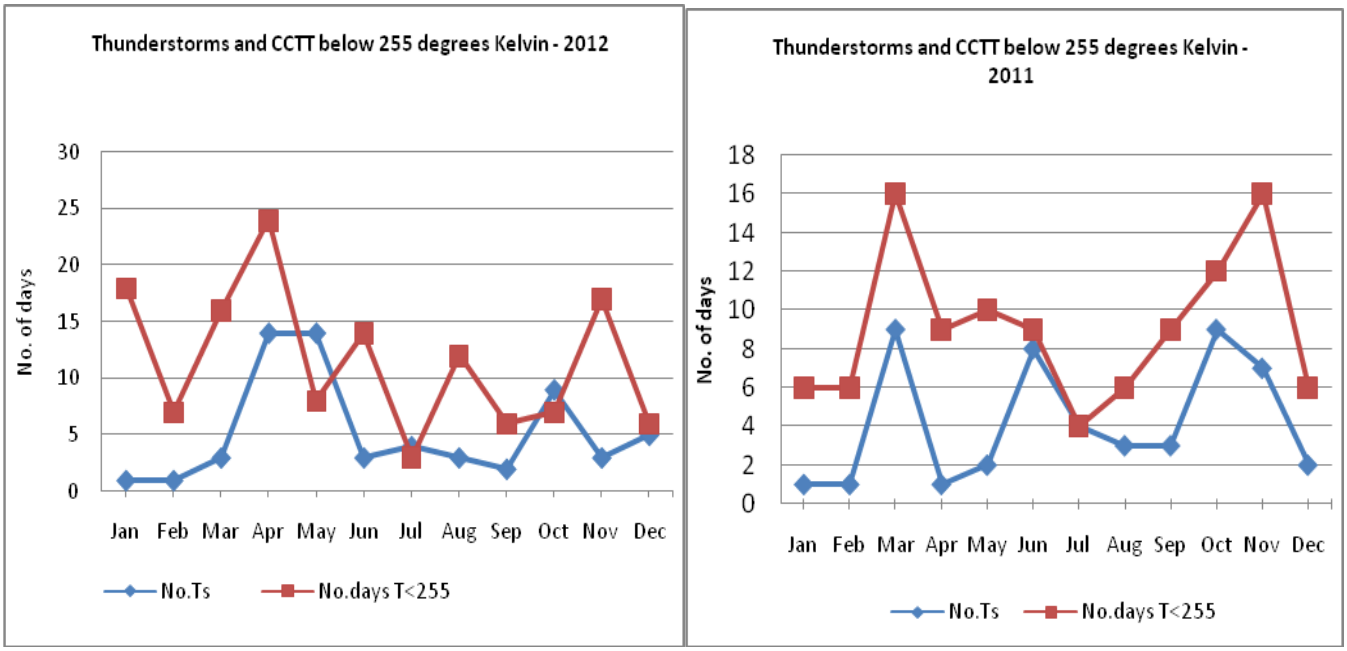

Fig.4.6: Nairobi Zone thunderstorms days associated with cold cloud top temperatures below 255 ${}^{0}K$

4.6 Results from Correlation Analysis

4.6.1 Correlation results between convective rainfall and Cold Cloud Top Temperatures

This section present and discusses the results of linear correlation between cold cloud top temperature and convective precipitation. Pearson correlation was performed to measure and interpret the strength of relationship between monthly Cold Cloud top temperature (CCTT) and convective precipitation from all the zones of study.

Correlation coefficient between monthly rainfall and cold cloud top temperatures during the period were summarized in figures 4.7, 4.8, 4.8 and 4.9 below.

Negative correlations indicated that as the cloud top temperature reduces, rainfall increases. This result was expected since rainfall increases with decreasing cloud tops temperatures. The highest magnitudes of correlation were observed over the region of study during the months of March to May and December.

The observed correlations may be linked to ITCZ migratory characteristics over the region which reflects the intensity of the convective systems.

Few cases of positive correlations were observed where the signals were affected by the daily episodic rains, durations and precipitation rates and duration and frequencies of CCTT threshold values.

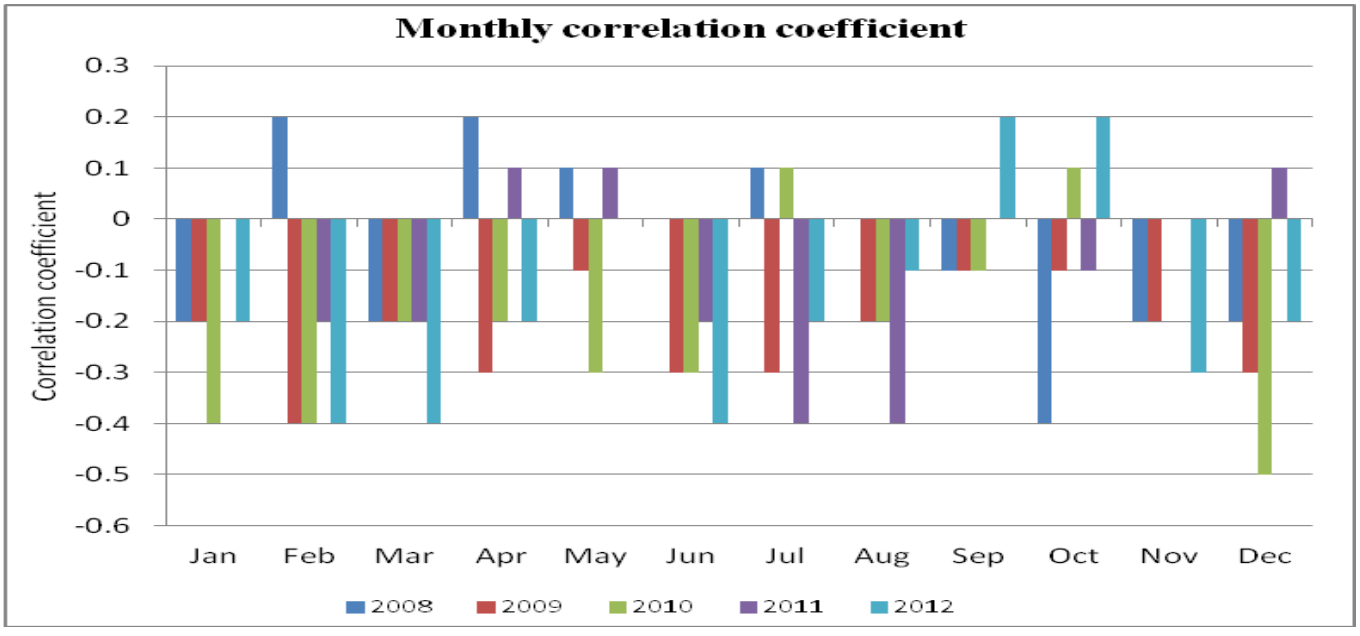

Fig.4.7: Lake Basin monthly correlation coefficients between convective rainfall and cold cloud top

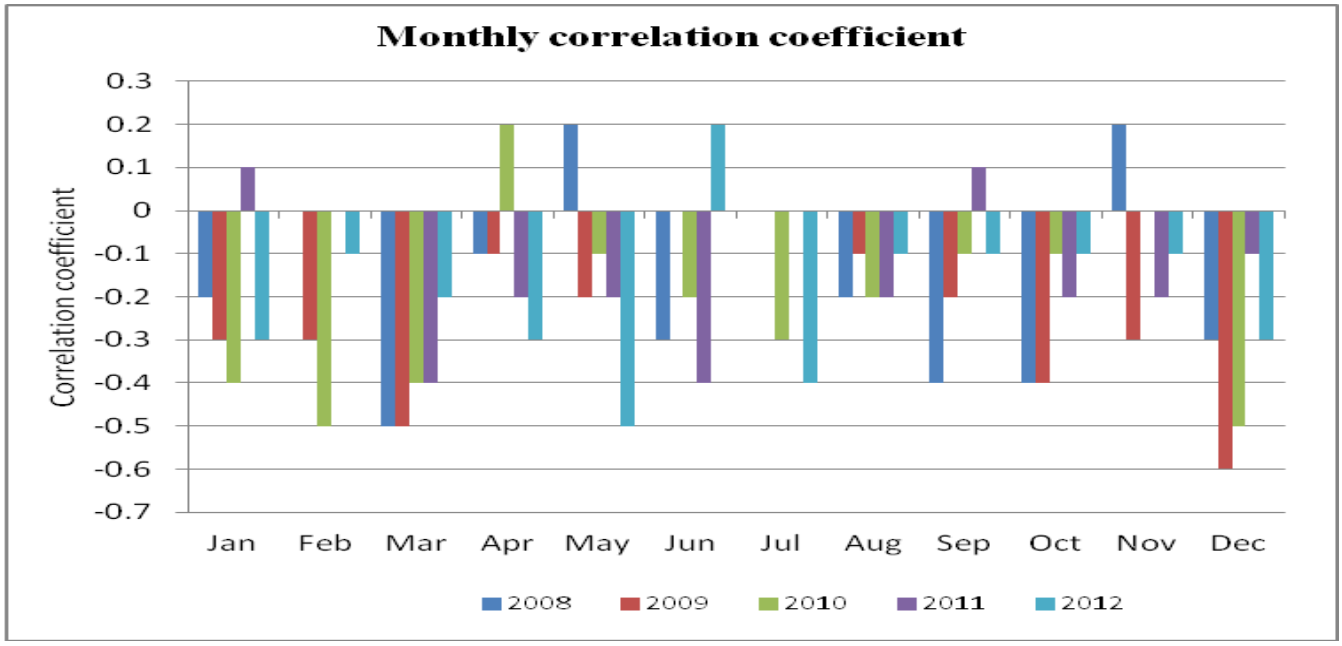

Fig.4.8: Western zone monthly correlation coefficients between convective rainfall and cold cloud top temperatures

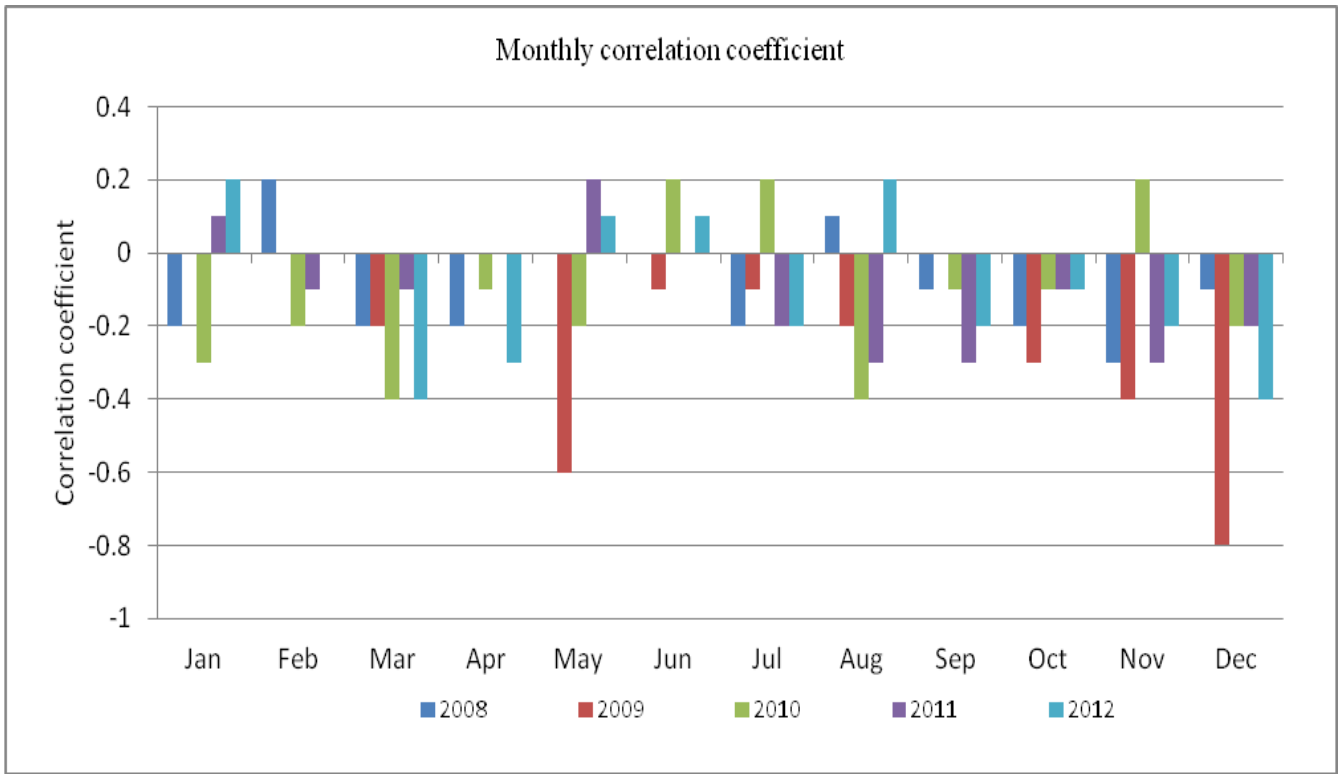

Fig.4.9: Central rift valley zone monthly correlation coefficients between convective rainfall and cold cloud top temperatures

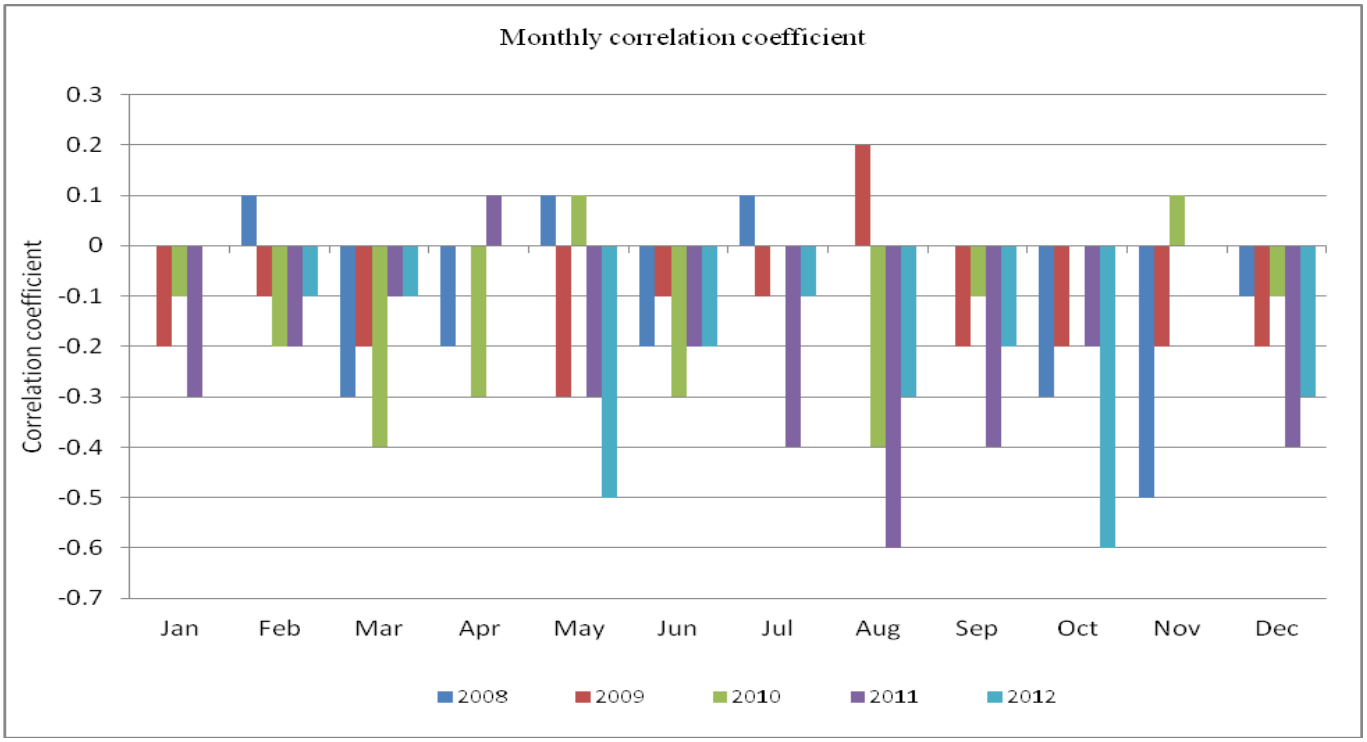

Fig.4.10: Nairobi zone monthly correlation coefficients between convective rainfall and cold cloud top temperatures

4.7 Analysis of winds circulation patterns

Figures 4.11, 4.12, 4.13and 4.14 indicates medium level winds at 1200z and 1500z on left and right panels respectively describing the convective motions which indicated trajectories and velocity of the deep convective systems associated with heavy rainfall over the region.

This is explained by winds circulations patterns indicating the influx of moisture from the Indian Ocean converging with Congo basin and Lake Victoria moisture coupled with local effects converging at the surface that induce vertical ascent of warm and less dense air resulting in convective activities.

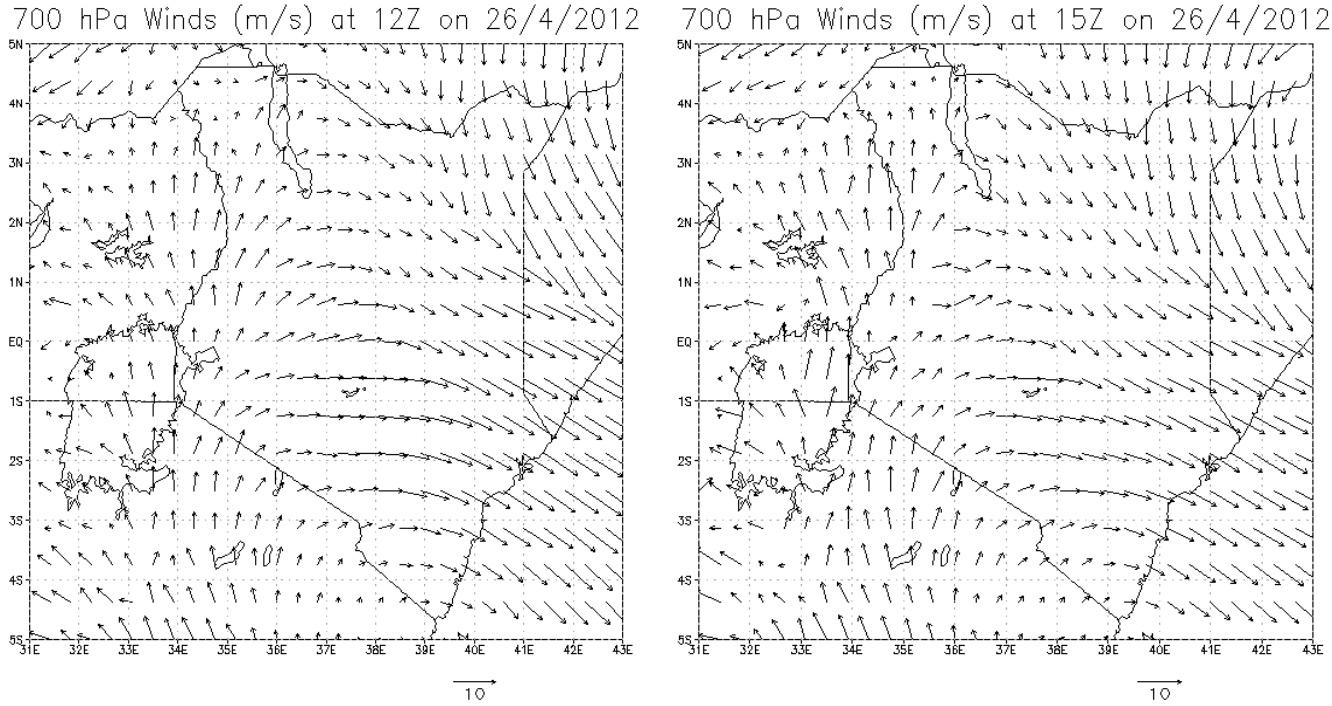

Fig.4.11: Medium level vector winds on 26th April, 2012

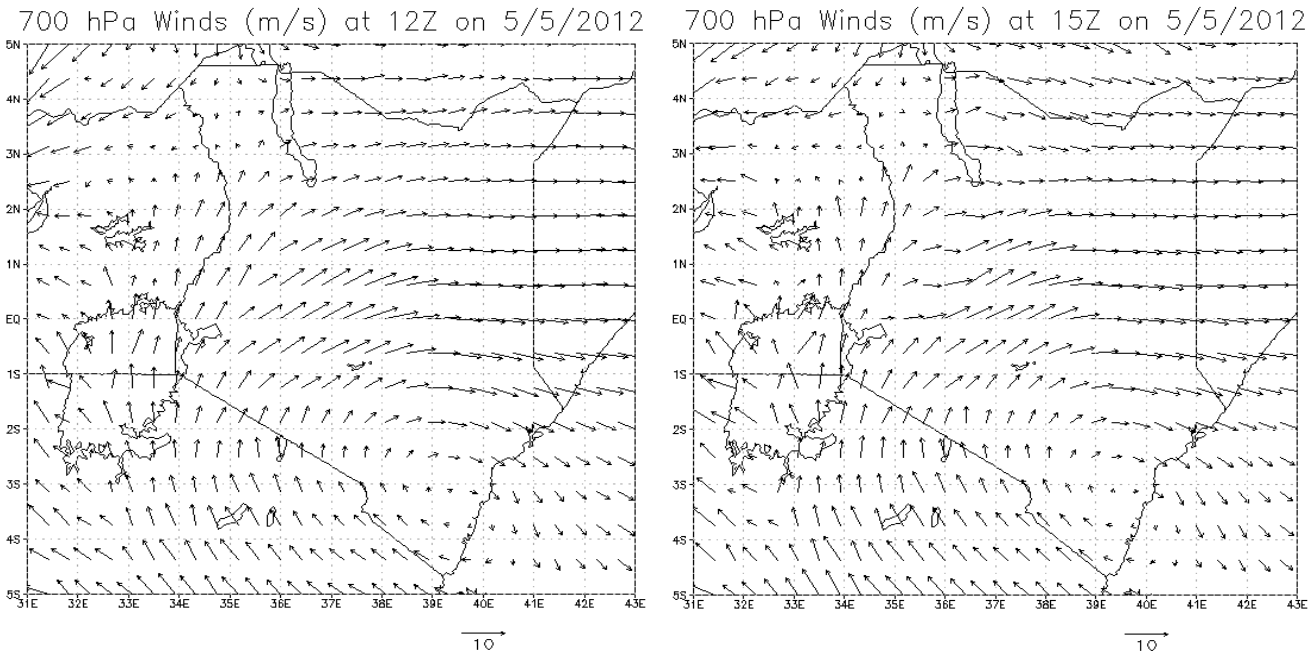

Fig.4.12: Medium level vector winds on 5th May,2012

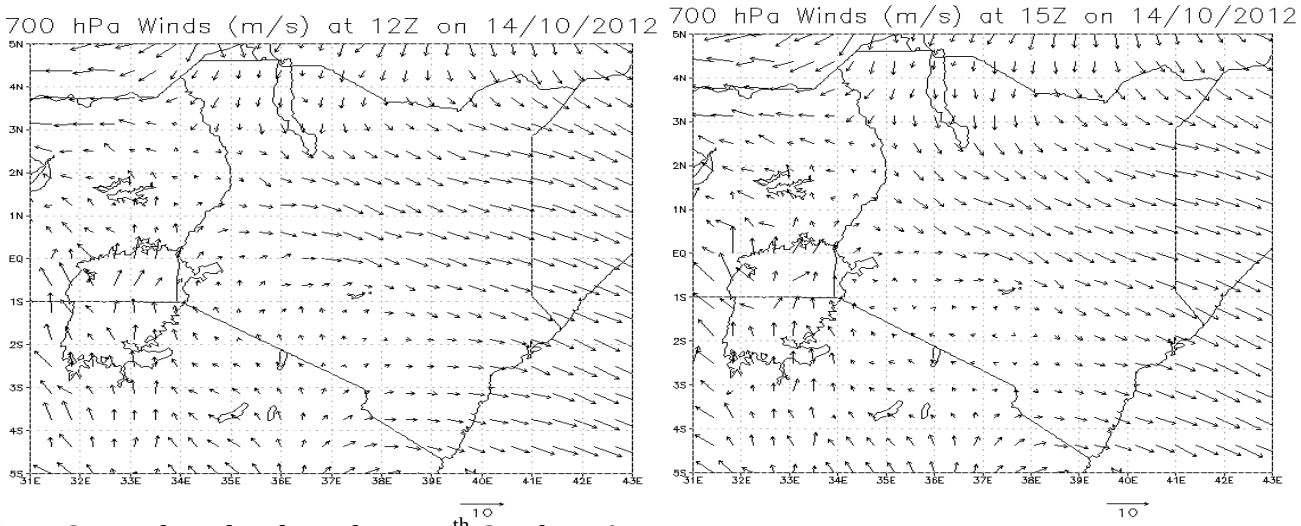

Fig.4.13: Medium level winds on 14th October 2012

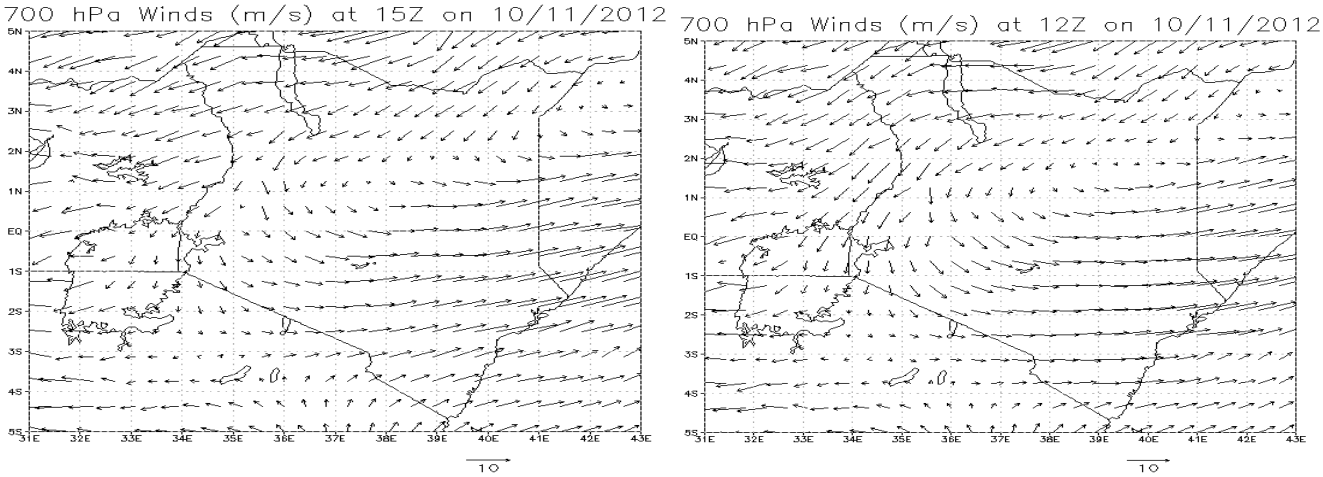

Fig.4.14: Medium level vector winds on 10th November ,2012

Table 4.11 shows the highest observed daily rainfall and CCTT over the zones associated with the effect of 700 hPa medium level winds during 2012 when heavy rainfall was experienced during the period.

Table 4.11: Highest Recorded Rainfall over the Zones Associated with the 700hPa Medium Level Winds during 2012

Months	**Region**	**Ppt (mm)**	**CCTT (Deg. Kelvin)**
April	Nairobi area zone	73.6	227.8
May	Western	88.0	196.3
October	Central Rift Valley	59.5	247.0
November	Lake basin	53.8	229.0

4.8 Results of assessment of aircraft costs related to adverse weather

The costs related to hazardous convective weather was estimated using computations by University of Westminster as indicated below. Table 4.12 indicates the distribution of the costs incurred due to delays as a result of adverse weather.

Table 4.12: Computation of aircraft costs per minute ($)

Item	Delay cost per minutes
Fuel costs	0
Maintenance costs	1
Crew costs	10
Airport charges	0
Aircraft ownership costs	-
Passenger compensation	24
Direct costs to an airline	36
Passenger opportunity costs	36

The data from Kenya Civil Aviation Authority revealed that over 200 aircrafts were delayed, diverted or, cancelled due to adverse convective weather especially by the national carrier Kenya Airways, other international airlines and local chartered flights to tourists' attraction areas like Maasai Mara.

Private Aircrafts for spraying agricultural large scale crops like tea bushes and wheat over Kericho and Narok respectively as well as transporting horticultural produce and fisheries from the region were adversely affected. These were estimated to costs billions of Kenya Shillings in lost earnings during the period.

The skilful prediction of convective systems as demonstrated in section 4.2 significantly reduce operating costs and lost passengers time as a result of convective hazards related aviation accidents/incidents, delays, diversions or cancellations.

Figures 4.15 below show time series in percentages of the aviation cost associated with convective precipitation indicating high cost during the months of May to May and October to December. Low aviation cost is observed over the months of January to February.

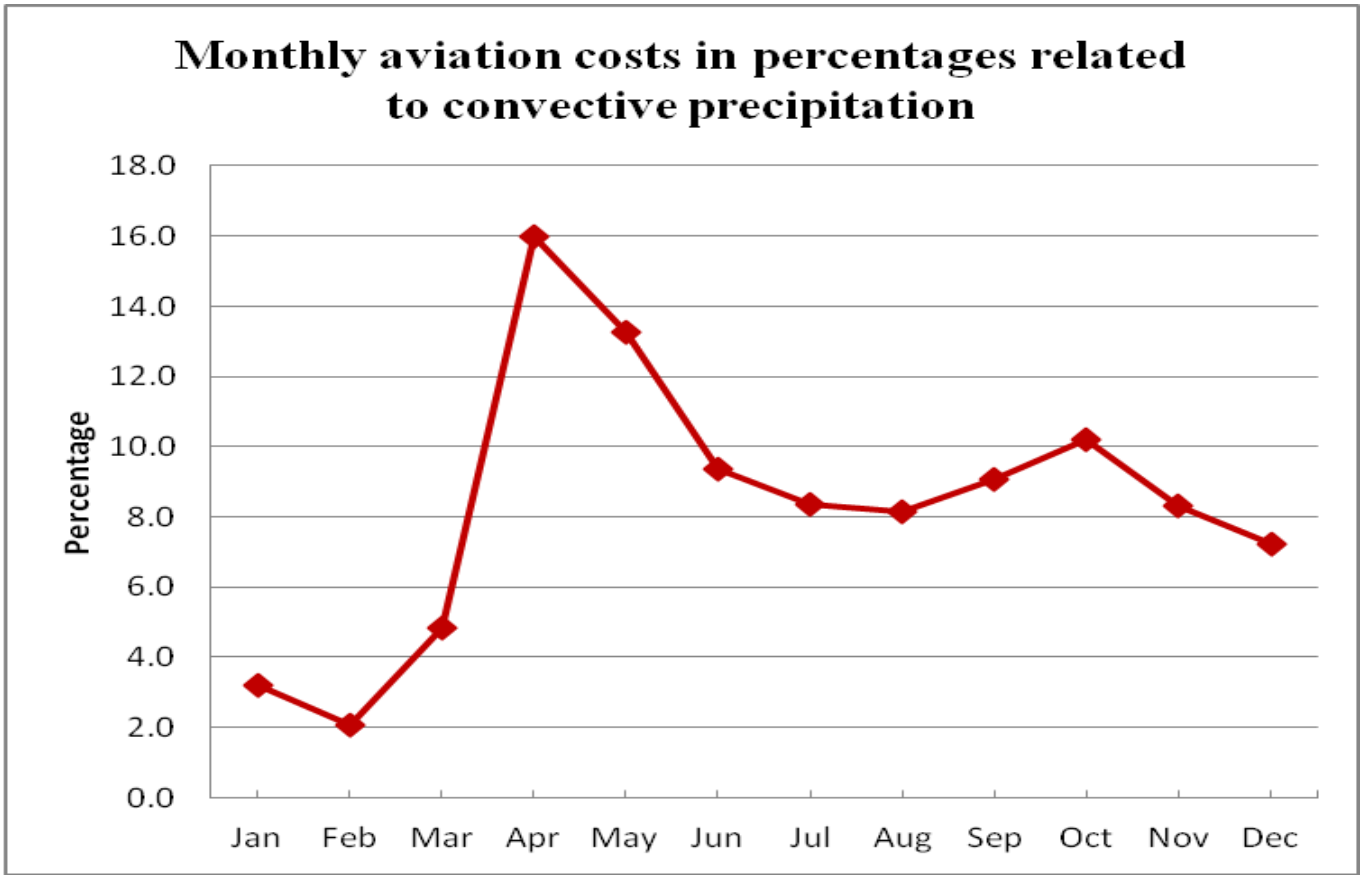

Fig. 4.15 Time series monthly aviation costs in percentages related to convective weather over the western part of Kenya.

The monthly distributions of the costs concurred with the trend of convective rainfalls over the region thus the diagnostic techniques can be used in planning of spatial and temporal distribution of aviation workload, for the management of air operations, terminal operations, regulations and suppression of the associated convective hazards.

It can be seen from figure 4.15 above that the cost associated with convective weather can be reduced through effective utilization of the CCTT threshold values in forecasting convective precipitation with high level of confidence as shown by high probability of detection in section 4.3.

CHAPTER FIVE

5.0 Summary, Conclusions and Recommendations

This chapter provides summary of the results obtained from various methods used to achieve the objectives of the study. The chapter also provides conclusions drawn and recommendations for further study.

5.1 Summary of the study

The dissertation was organized into five main chapters.

Chapter one introduced the challenges of forecasting convective weather, the area of study, relief characterizing the region as well as the physical features which influence its weather. The climate of the region was discussed at length as well as the rainfall regimes in the region. The major seasons influencing aviation over the region were examined either, including a highlight on the section of the aviation weather hazards.

Large scale systems affecting weather over the region were explored and the most important ones were highlighted including ITCZ, QBO, ENSO, MJO, monsoons, tropical cyclones, jet streams, subtropical highs, and easterly/westerly waves among other features.

The socio-economic challenges posed by erratic weather events to aviation industry over the region were considered together with solutions that need to be sought in order to address these challenges. The problem being investigated in the study was mentioned.

The overall objective of the study was to investigate the nowcasting predictability of convective rainfall over western Kenya using satellite infrared 10.8 μm band cold cloud top temperatures. This included quantifying significant cloud top temperatures associated with convective rainfall with the aim of determining threshold values associated with convective rainfall. Although numerous similar studies have been carried out, very little has been done not only in western Kenya but in Equatorial regions over East Africa in related studies.

Chapter two provides a framework for discussion of the relevant cold cloud top temperature threshold values which have been developed to characterize convective storms. Infrared cloud top temperature measurements allows detection of changes in the temperature of clouds during the day and at night with deep convective clouds being inversely proportional to the temperature, warm temperatures are dark and cold temperatures are lighter.

Based on the interpretation by the satellite instruments of the electromagnetic (EM) radiation scattered or emitted (Thies et al. 2008a) the satellite information are used as a proxy for convective rainfalls.

Chapter two also discusses the effect of convective weather on the aviation industry with the emphasis of hazardous weather on different phases of flights.

Chapter three described the data and methodologies adopted for the study. The data used in this study included daily rainfall and associated convective phenomena from ten synoptic stations representing the regions and daily archived coldest cloud top temperature data of the same temporal and spatial resolution from 2008 to 2012.

The gridded wind data at the 700hpa level and 500hpa (*u* and *v*) extracted from COSMO Model archives during 2012 was used to describe the divergence/vertical motions.

Observed rainfall data, wind and other associated convective phenomena were provided by the Kenya Meteorological Services while cloud top temperatures were acquired from European Meteorological Satellite Centre at website http://www.eumetsat.int/Home/Main/DataAccess/EUMETSAT Data Centre.

Kenya Civil Aviation Authority provided the operational flight data on adverse convective precipitation.

The methodology involved matching the satellite data spatially and temporally with the convective rainfall events from the same geographical coordinate pixel points.

The homogeneous zones for study area were done according to climatic conditions of the area based on Principal Component Analysis (Ogallo, 1980; 1988, Basalirwa 1993, Indeje *et al* 2000) to capture rainfall stations which have similar temporal characteristics. The thresholds Cold Cloud Top Temperatures between $T_1 = -18^0 c = 255^0 K$ and $T_2 = -78^0 c = 195^0 k$ were defined to separate the cold cloud and thick cirrus associated with convective rainfall that constitute the coldest events observed by satellite.

The predictability of convective precipitation using cloud top temperature indices was done to investigate the predictability potential using statistical methods. Contingent tables were constructed to assess the predictability of daily rainfall over the region during the year for the months of January and February (JF), May, April and May (MAM), June, July, August and September (JJAS) and October, November and December (OND) for the purposes of evaluating the skill scores using the derived CCTT indices.

Last but not least the economic impacts of the adverse convective rainfall on aviation industry over the region were assessed using the previous studies (Sands *et al*, 2009; Warren, 2009; Muiruri, 2011).

5.2 Results of the Study

To identify cloud top temperature values associated with convective rainfall, tables, graphs, charts and other statistical methods were used. The results indicated that most convective rainfall from all the zones occurred between clouds top temperatures 235^0K to 255^0K with the highest probability of detection at 90% over western zone during the month of April long rainy season.

The other zones recorded over 60% probability of detection of convective rainfall during the same month. The lowest probability of detection occurred during January, February, June, July, August and September over all the four zones as indicated by the time series analysis.

Pearson products correlation coefficient was highest over Western zones with cc of -0.8 indicating that as the cloud top temperature reduces, rainfall events increases and vise versa. From the examination of the skill scores, the highest hit scores were during the rainy seasons with the highest misses during dry season. This is due to longitudinal migration of the Inter Tropical Convergence Zone (ITCZ), which is the main rainfall generating system caused by convergence between the southeasterly and northeasterly monsoons generated by the sub tropical anticyclones both in the northern hemisphere (Azores and Arabian ridge) and southern hemisphere (St Helena and Mascarene).

The result from time series analysis also indicated positive correlations between CCTT and highest number of thunderstorm days during the MAM over central rift valley represented by Kericho area due to the convergence of moist air masses from Lake Victoria with the MAU forest and other local effects conducive for the development of convective activities.

From medium level winds analysis at 700 hPa and 500 hPa levels, the results depicted a diffluent flow on the lake shores when heavy rainfall days were observed during the months of April, May, October and November. This is explained by winds circulations indicating the influx of moisture from the Indian Ocean converging with Congo basin and Lake Victoria moisture coupled with local effects.

This therefore induce vertical ascent of warm and less dense air in the equatorial trough. Going by the law of mass conservation (the continuity equation), horizontal velocity convergence of winds at the surface induces upward movement of air. This would normally result in cloudiness in the vicinity of the convergence zone but only if certain conditions are fulfilled including availability of sufficient moisture, presence of physical features like mountains as well as large water bodies which accentuate instability.

Adverse weather impacted losses to lives, socio and economic losses to the aviation industry resulting into the dead of Roads Minister Kipkalya Kones, Assistant Home Affairs Minister Lorna Laboso, pilot and a bodyguard in 2008 in the afternoon hours around Mau forest areas (*Daily Nation,* 11 June 2008).

Chapter five was dedicated towards summarizing the entire dissertation and providing the conclusions drawn as well as recommendations for the utilization of the products obtained. Recommendations for further works were also enunciated under the same chapter.

5.3 Conclusions

The main purpose of this study was to investigate infra red cloud top temperature threshold values associated with convective precipitation. The derived indices, namely the cold cloud top temperature (CCTT) indices have effectively characterized the convective rainfall over the region.

Significant negative correlations were observed between the convective rainfall and the cold cloud top temperature indices which indicated that as the cloud top temperature reduces, the convective systems deepened thus increasing the precipitable water signaling the depth of water in a column of the atmosphere that would precipitate as rain over the region.

The correlations suggested that the indices could be used with other indices to improve the short range predictions and this is supported by the skill scores which indicated relationship between convective rainfall and the cold cloud top temperatures.

The trend test indicated the behavior of the cold cloud top temperature is distinct during the wet seasons in particular MAM and OND long rainy seasons and weak during dry seasons.

The medium level winds circulation patterns at 700 hPa can be used as one of the ingredients of analyzing trajectories and velocities of convective systems in improving the aviation weather forecasts over the western part of Kenya.

The diagnostic and short range forecasting techniques of using CCTT indices with 75 percent confidence level of probability of detection can be utilized in the management of aviation industry by taking advantages of forecasted convective systems in reducing operational costs, loss of lives and socio-economic impacts associated with hazardous convective weather over the region.

5.4 Recommendations

The study has shown that indices of cloud top temperatures can characterize convective rainfall based on the significant correlations obtained. The following are the recommendations resulting from the study made:

- The CCTT threshold indices can be incorporated in the interest of improving nowcasting predictability skills.
- Satellite data to be used alongside others to enhance weather information over remote areas and sparse meteorological observing systems in improving short range predictions.
- Research in development of new tools for improving weather and climate monitoring systems is essential in achieving the millennium development goals in Kenya by ensuring environmental sustainability.
- Further studies are to be carried out on predictability of short range forecasting using satellite derived information in designing models used to estimate precipitation.

References

Adler, R. F., M. J. Markus, and D. D. Fenn, 1985: Detection of severe Midwest thunderstorms using Geosynchronous satellite data. Monthly Weather Review, **113**, 769-781

Asnani, G.C., 2005: Tropical Meteorology. Prof G.C. Asnani, 822, Sindh colony, Aundh, Pune, India **Vol 1**. 1202pp.

Bedka, K., J. Brunner, R. Dworak, W. Feltz, J. Otkin, and T. Greenwald, 2010: Objective Satellite-Based Detection of Overshooting Tops Using Infrared Window Channel Brightness Temperature Gradients. *J. Appl. Meteor. Climatol.*, **49**, 181–202.

Bedka, K, R. Dworak, J. Brunner, and W. Feltz, 2010: Validation of Satellite-Based Objective Overshooting Top Detection Methods Using Cloud Sat Cloud Profiling Radar Observations, *J. Appl. Meteor*. Climatol. In preparation for *J. Appl. Meteor*. Climatol.

Brunner, J.C., S.A. Ackerman, A.S. Bachmeier, and R.M. Rabin, 2007: A Quantitative Analysis of the Enhanced-V Feature in Relation to Severe Weather. Wea. Forecasting, **22**, 853–872.

Camberlin, P., & Okoola, R. E. (2003) The Onset and cessation of the "long rains" in Eastern Africa and their interannual variability. Theor. Appl. Climatol. 75, 43-54, doi: 10.1007/s00704-002-0721-5.

Carbone, R. E., J. D. Tuttle, D. Ahijevych, and S. B. Trier, 2002: Inferences of predictability associated with warm season precipitation episodes. *J. Atmos. Sci.*, **59**, 2033–2056.

Heymfield, G.M and Fulton ,R.Microphysical and radiative characteristics of convective clouds during COHMEX. *J. Appl. Meteorol*.,**30**,98-116

Heymsfield, G. M., G. Szejwach, S. Schotz, and R.H. Blackmer, Jr., 1983: Upper level structure of Oklahoma tornadic storms on 2 May 1979, Pt. 2 Proposed explanation of "V" pattern and internal warm region in infrared observations. Journal of Atmospheric Science, **40**, 1756-1767.

H. Feidas and C. Cartalis. Monitoring mesoscale convective cloud systems associated with heavy storms with the use of Meteosat imagery.*Journal of Applied Meteorology*, **40**:491–512, 2001.

Hutchison, K., 1999: Application of AVHRR/3 imagery for the improved detection of thin cirrus clouds and specification of cloud-top phase. *J. Atm. Oceanic* Tech., **16**, 1885-1899.

Indeje, M., F. H. M. Semazzi, and Laban J. Ogallo, 2000: ENSO signals in East African rainfall seasons. *Int. J. Climatol*. **20**: 19–46.

Ininda, J. M, 1998, "Simulation of the impact of sea surface temperature anomalies on the short rains over East Africa", *J. African Meteo.* Soc., **3**, 1, 127-140.

Jackson, B., S. E. Nicholson, and D. Klotter, 2009: Mesoscale convective systems over western equatorial Africa and their relationship to large-scale circulation. *Mon. Wea. Rev.*, **137**, 1272–1294.

Kidder, S., Kankiewicz, J.A., Eis, K. (2005): Meteosat Second Generation cloud algorithms for use in AFWA. In BACIMO 2005, Monterey, CA.

Laing ,A,G and Carbone,R,E (2011):Cycles and propagation of deep convection over the equatorial Africa.*Mon Wea Rev*.**Vol 139**,2832-2853;″MJO impacts''P2052

Liang Ping, Tang Xu, He Jin-Hai , Chen Long-Xun, 2008: An East Asian subtropical summer monsoon index defined by moisture transport, *Journal of Tropical Meteorology*, **14** *No.1, pg 61-64*

Lakshmanan, V., T. Smith, G. Stumpf, and K. Hondl, 2007: The Warning Decision Support System–Integrated Information. *Wea. Forecasting*, **22**, 596–612.

Machado, L.A.T., and H. Laurent, 2004: The Convective System Area Expansion over Amazonia and Its Relationships with Convective System Life Duration and High-Level Wind Divergence. *Mon. Wea. Rev.*, **132**, 714–725.

McDonough, F. and B. C. Bernstein: Combining satellite, radar, and surface observations with model data to create a better aircraft icing diagnosis. Preprints, 8th Conf. On Aviation, Range, and Aerospace Meteorology, Dallas, TX, *Amer. Meteor. Soc*., **467**-471.

Mecikalski, JR., Bedka, KM., (2006) Forecasting convective initiation by monitoring the evolution of moving cumulus in daytime GOES imagery. *Mon Wea Rev* **134**: 49-68

Mecikalski, J. R., D. B. Johnson, J. J. Murray, and many others at UW-CIMSS and NCAR, 2002: NASA Advanced Satellite Aviation-weather Products (ASAP) study report. NASA Tech. Rep., 65 pp. [Available from the Schwerdtferger Library, 1225 West Dayton Street, University of Wisconsin-Madison, Madison, WI 53706.]

Medlin, J. M., and P. J. Croft, 1998: A preliminary investigation and diagnosis of weak shear summertime convective initiation for extreme southwest Alabama. Wea. Forecasting, **13**, 717–728.

Miner, C., S. Abelman, and J. Stobie, 2009. Building a 4-D weather data cube for 2013 IOC. *Aviation, Range and Aerospace Meteorology Special Symposium on Weather-Air Traffic Management Integration*, 13 January 2009, Phoenix, AZ, American Meteorological Society

Mueller, C. K., J. W. Wilson, and N. A. Crook, 1993: The utility of sounding and mesonet data to nowcast thunderstorm initiation.Wea. Forecasting,**8**,132–146

Murray, J. J., 2002: Aviation weather applications of Earth Science Enterprise data. Earth Observation Magazine, Vol. **11**, No. 8, GITC America, 27–30.

Mutai, C. C., M.N. Ward and A.W Coleman, 1998:Towards the prediction of the East Africa short rains based on sea-surface temperature-atmosphere coupling.*Int. J. Climatol*.**18**, 975-997

Nair, U. S., R. C. Weger, K. S. Kuo, and R. M. Welch, 1998: Clustering, randomness, and regularity in cloud fields. 5. The nature of regular cumulus cloud fields. *J. Geophys. Res*, **103**, 11 363–11 380.

Ogallo, L. J., 1980: Rainfall variability in Africa. *Mon. Wea. Rev*. **107:**1133-1139.

Ogallo, L. J., Janowiak, J. E. and Halpert, M. S., 1988: Teleconnection between seasonal rainfall over East Africa and Global seas surface temperature anomalies. *J. Met. Soc. Jpn*. **66**:807-822

Okoola. RE (1998) spatial evolution of the active convective patterns across the equatorial eastern Africa region during Northern Hemisphere spring season using outgoing radiation records. *Meteorol Atmos Phys* **66**:51-63.

Petersen, R. A., R. Aune, T. Rink, 2010: Objective short-range forecasts of the pre-convective Environment using SEVIRI data, EUMETSAT Conference, Cordoba, Spain

Politovich, M.K., 1993: Aircraft Icing: Meteorological Effects on Aircraft Performance. Proceedings, Fifth International Conference on Aviation Weather Systems, *Aug.2-6, 1993,* Vienna, Va.

Rosenfeld, D., and W. L. Woodley (2000), Deep convective clouds with sustained super cooled liquid water down to 37.5 C, Nature,405, 440–442.

Sasse, M. and Hauf, T. (2003) A study of thunderstorm-induced delays at Frankfurt Airport, Germany Meteorological Applications 10(1), 21-30

Schumacher, C, and RA Houze, Jr. 2003. "Stratiform rain in the tropics as seen by the TRMM precipitation radar." *Journal of Climate* **16**.

Sieglaff, J., L. Cronce, W. Feltz, K. Bedka, M. Pavolonis, and A. Heidinger, 2010: Nowcasting convective Storm Initiation Using Satellite Based Box-Averaged Cloud Top Cooling and Cloud Type Trends. Submitted to *J. Appl. Meteor. Climatol*.

Thies, B., Nauss T., Bendix J., (2008b) A new technique for detecting precipitation at mid latitudes during daytime using Meteosat Second Generation SEVIRI. 2008 EUMETSAT Meteorological Satellite Conference, Darmstadt, Germany

Thies, B., Nauss T, Bendix J., (2008a) Discriminating raining from non raining cloud areas at mid latitudes using meteosat second generation SEVIRI night time data. *J. Appl. Meteor*, **15**, 219-230

Tomsett A.C and Ralf Toum..(1994) Diurnal temperature range and rainfall probability over united kingdom

Wan T. and Wu S. W., "Aerodynamic Analysis under Influence of Heavy Rain," *Journal of Aeronautics, Astronautics, and Aviation*, vol**. 41**, No.3, September 2009, pp.173-180.

Appendices

Appendix A; Plots
Zonal Winds associated with heavy rainfall during April, May, October and November 2012

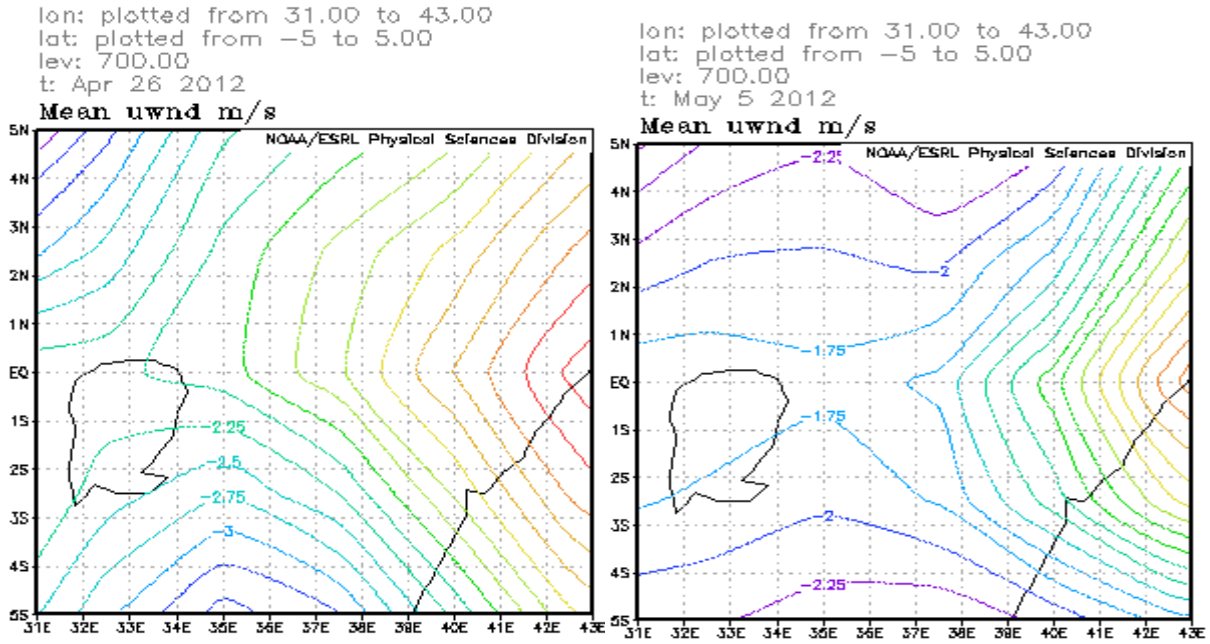

700hpa zonal winds during April and May, 2012 on left and right panels respectively.

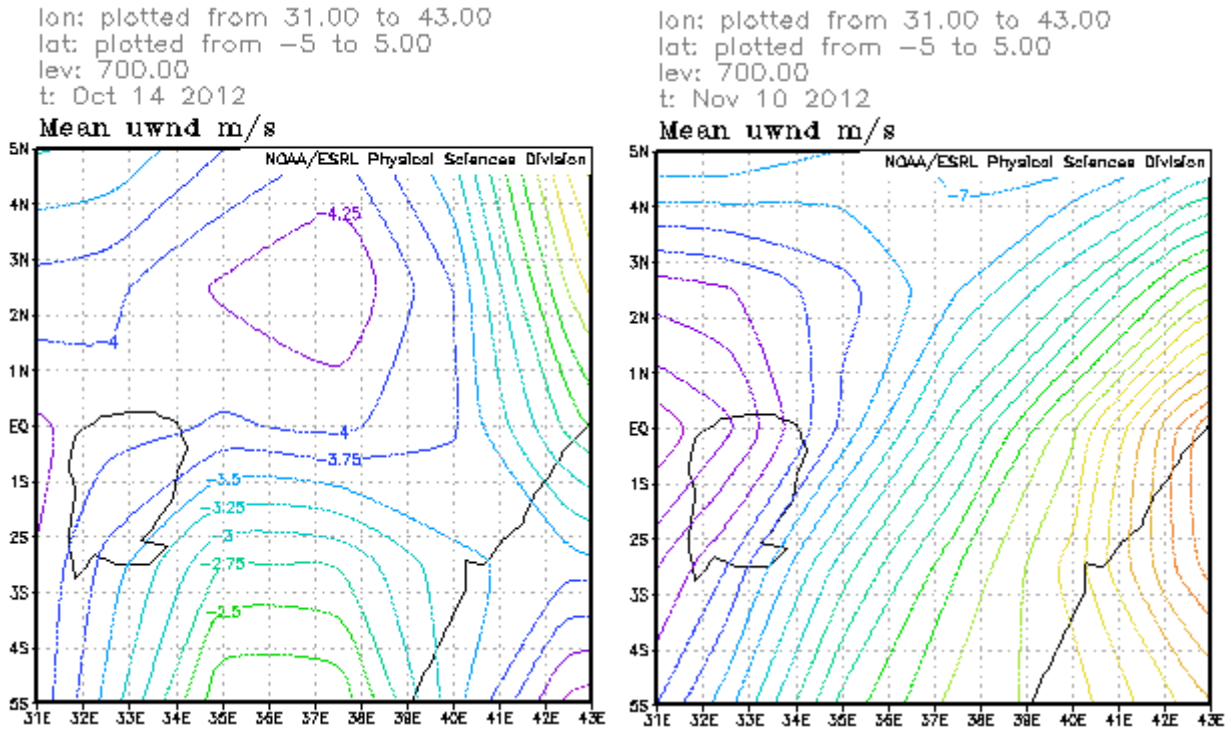

700hpa zonal winds during October and November, 2012 on left and right panels respectively.

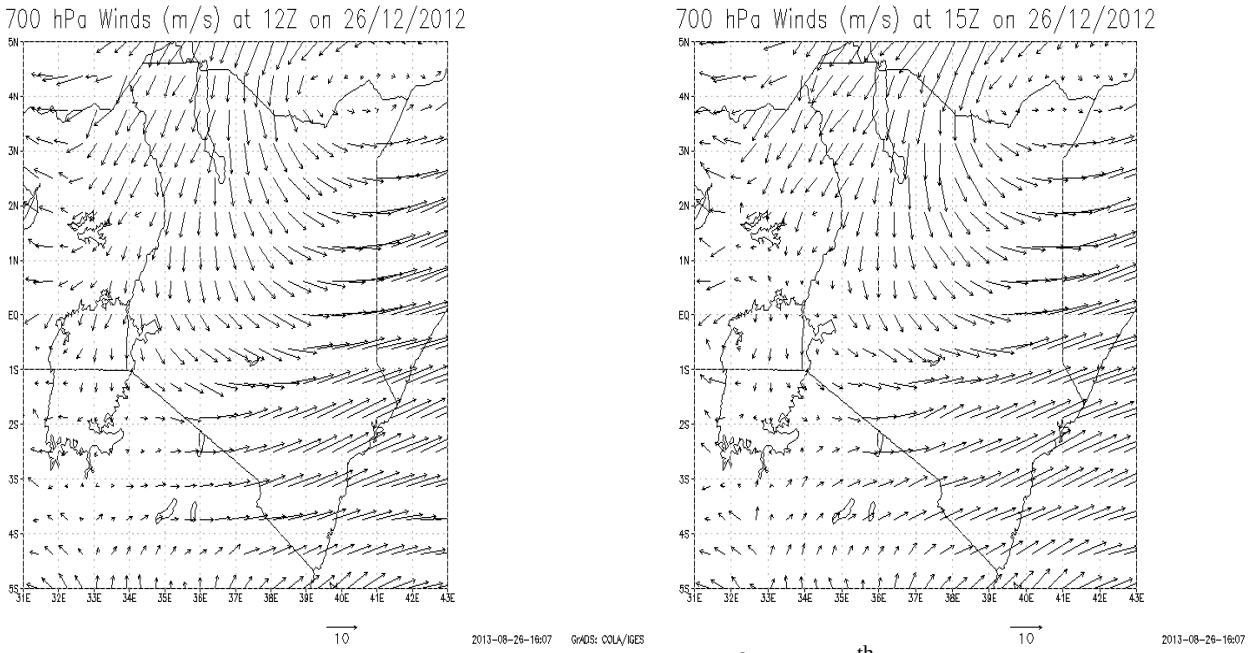

Medium level vector wind associated with heavy convective rainfall on 26th December 2012

Appendix B: Tables

B 1: Thunderstorm days

B 1.1: Number of thunderstorms days observed over the stations during 2012

Months	Kericho	Nakuru	Narok	Kisii	Kisumu	Kakamega	Kitale	Eldoret	JKIA	Wilson A/P
Jan	9	6	8	6	3	4	3	2	1	1
Feb	8	4	3	5	7	4	1	1	0	0
Mar	13	4	6	12	8	8	2	1	1	2
Apr	**27**	16	13	**18**	23	23	25	16	8	5
May	**26**	11	7	**25**	17	27	24	16	5	3
Jun	21	11	3	20	16	16	26	21	1	1
Jul	19	18	3	14	9	13	21	22	1	1
Aug	21	10	2	15	14	15	19	17	1	1
Sep	20	18	1	18	19	19	16	15	1	1
Oct	17	16	4	16	19	24	16	5	3	3
Nov	18	9	6	16	17	18	13	6	2	2
Dec	15	13	15	13	9	9	7	6	3	2
Total	**216**	**136**	**71**	**178**	**161**	**180**	**173**	**128**	**27**	**22**

B 1.2: Number of thunderstorms days observed during 2011

Months	Kericho	Nakuru	Narok	Kisii	Kisumu	Kakamega	Kitale	Eldoret	JKIA	Wilson A/P
Jan	9	5	7	5	4	4	2	3	0	0
Feb	9	4	6	4	4	3	2	2	1	0
Mar	19	4	14	21	17	19	14	6	3	3
Apr	18	11	2	19	14	17	11	8	1	1
May	27	10	3	23	19	23	19	16	3	1
Jun	23	17	6	21	22	18	23	21	1	2
Jul	20	16	4	17	15	16	20	20	1	1
Aug	21	11	1	19	12	17	19	21	1	1
Sep	20	12	3	24	19	14	19	16	1	2
Oct	18	12	1	23	16	15	12	11	3	2
Nov	18	4	7	16	19	13	16	10	4	3
Dec	12	12	15	12	7	9	2	1	1	1
Total	**214**	**118**	**69**	**204**	**168**	**168**	**159**	**135**	**20**	**17**

B 2.0: Contingence table

Observed rainfall category	***CCTT threshold category***		
	Yes :CCTT $\leq 255\ ^{0}K$	***No:*** CCTT $\geq 255\ ^{0}K$	Marginal total
Yes: Rain	Hits	Misses	Observed Yes
No rain	False alarm	Correct negatives	Observed No
Marginal total	Yes: Threshold values	No signal	Total

Observed rainfall category	***CCTT threshold category***		
	Yes	***No***	Marginal total
Rain (Yes)	a	b	a + b
No rain	c	d	c + d
Marginal total	a + c	b+ d	a + b + c + d

$$POD = \frac{hits}{hits + misses}$$

Hit rate = $\frac{a}{(a+c)}$

False alarm = $\frac{c}{(a+c)}$

B 2.1: Simple scores for central rift valley

Months	Observed rainfall days	Hits	Misses	False alarms	Correct Negative	Probability of Detection
Jan	54	18	46	33	58	**0.3**
Feb	60	28	33	40	38	**0.5**
Mar	88	68	20	32	35	**0.8**
Apr	134	85	49	16	5	**0.6**
May	131	68	63	10	14	**0.5**
Jun	111	33	78	12	32	**0.3**
Jul	124	47	77	7	24	**0.4**
Aug	132	36	96	4	19	**0.3**
Sep	130	42	88	9	16	**0.3**
Oct	136	66	70	13	6	**0.5**
Nov	110	67	43	17	28	**0.6**
Dec	67	36	31	18	70	**0.5**

B 2.2: scores for Nairobi zone

Months	Observed rainfall days	Hits	Misses	False alarms	Correct Negative	Probability of Detection
Jan	19	3	14	28	107	0.2
Feb	32	11	21	21	83	0.3
Mar	68	51	17	36	51	0.8
Apr	107	66	41	17	31	0.6
May	101	32	69	19	35	0.3
Jun	57	12	45	23	75	0.2
Jul	50	10	40	16	89	0.2
Aug	66	15	51	16	73	0.2
Sep	45	9	36	28	82	0.2
Oct	58	31	27	22	75	0.5
Nov	100	50	50	21	34	0.5
Dec	76	22	54	17	62	0.3

B 2.3: Simple scores for Lake Basin zone

Months	Observed rainfall days	Hits	Misses	False alarms	Correct Negative	Probability of Detection
Jan	55	28	27	35	65	0.5
Feb	70	40	30	27	43	0.6
Mar	105	66	39	23	27	0.6
Apr	127	86	41	20	8	0.7
May	126	66	60	11	18	0.5
Jun	106	44	62	6	43	0.4
Jul	80	19	61	15	60	0.2
Aug	100	23	77	10	45	0.2
Sep	130	45	85	7	18	0.3
Oct	116	61	55	13	26	0.5
Nov	114	70	44	12	29	0.6
Dec	109	51	58	8	38	0.5

B 2.3: Simple scores for Western zone

Months	Observed rainfall days	Hits	Misses	False alarms	Correct Negative	Probability of Detection
Jan	45	15	30	36	68	0.3
Feb	41	31	20	38	51	0.8
Mar	89	69	20	26	40	0.8
Apr	117	102	15	18	20	0.9
May	135	91	44	9	11	0.7
Jun	126	54	72	6	23	0.4
Jul	137	47	90	6	12	0.3
Aug	141	45	96	4	10	0.3
Sep	139	66	73	6	10	0.5
Oct	129	72	57	7	19	0.6
Nov	96	67	29	25	34	0.7
Dec	62	40	22	20	73	0.6

B 3: Regional Correlation coefficients

B 3.1: Correlation coefficients during 2008

Months	Lake basin	Western	Central rift valley	Nairobi zone
Jan	-0.2	-0.2	-0.2	0
Feb	0.2	0	0.2	0.1
Mar	-0.2	-0.5	-0.2	-0.3
Apr	0.2	-0.1	-0.2	-0.2
May	0.1	0.2	0	0.1
Jun	0	-0.3	0	-0.2
Jul	0.1	0	-0.2	0.1
Aug	0	-0.2	0.1	0
Sep	-0.1	-0.4	-0.1	0
Oct	-0.4	-0.4	-0.2	-0.3
Nov	-0.2	0.2	-0.3	-0.5
Dec	-0.2	-0.3	-0.1	-0.1

B 3.2: Correlation coefficients during 2009

Months	Lake basin	Western	Central rift valley	Nairobi zone
Jan	-0.2	-0.3	0	-0.2
Feb	-0.4	-0.3	0	-0.1
Mar	-0.2	-0.5	-0.2	-0.2
Apr	-0.3	-0.1	0	0
May	-0.1	-0.2	-0.6	-0.3
Jun	-0.3	0	-0.1	-0.1
Jul	-0.3	0	-0.1	-0.1
Aug	-0.2	-0.1	-0.2	0.2
Sep	-0.1	-0.2	0	-0.2
Oct	-0.1	-0.4	-0.3	-0.2
Nov	-0.2	-0.3	-0.4	-0.2
Dec	-0.3	-0.6	-0.8	-0.2

B 3.3: Correlation coefficients during 2010

Months	Lake basin	western	Central rift valley	Nairobi zone
Jan	0.4	-0.4	-0.3	-0.1
Feb	-0.4	-0.5	-0.2	-0.2
Mar	-0.2	-0.4	-0.4	-0.4
Apr	-0.2	0.2	-0.1	-0.3
May	-0.3	-0.1	-0.2	0.1
Jun	-0.3	-0.2	0.2	-0.3
Jul	0.1	-0.3	0.2	0
Aug	-0.2	-0.2	-0.4	-0.4
Sep	-0.1	-0.1	-0.1	-0.1
Oct	0.1	-0.1	-0.1	0
Nov	0	0	0.2	0.1
Dec	-0.5	-0.5	-0.2	-0.1

B 3.4: Correlation coefficients during 2011

Months	Lake basin	Western	Central rift valley	Nairobi zone
Jan	0	0.1	0.1	-0.3
Feb	-0.2	0	-0.1	-0.2
Mar	-0.2	-0.4	-0.1	-0.1
Apr	0.1	-0.2	0	0.1
May	0.1	-0.2	0.2	-0.3
Jun	-0.2	-0.4	0	-0.2
Jul	-0.4	0	-0.2	-0.4
Aug	-0.4	-0.2	-0.3	-0.6
Sep	0	0.1	-0.3	-0.4
Oct	-0.1	-0.2	-0.1	-0.2
Nov	0	-0.2	-0.3	0
Dec	0.1	-0.1	-0.2	-0.4

B 3.5: Correlation coefficients during 2012

Months	Lake basin	western	Central rift valley	Nairobi zone
Jan	-0.2	-0.3	0.2	0
Feb	-0.4	-0.1	0	-0.1
Mar	-0.4	-0.2	-0.4	-0.1
Apr	-0.2	-0.3	-0.3	0
May	0	-0.5	0.1	-0.5
Jun	-0.4	0.2	0.1	-0.2
Jul	-0.2	-0.4	-0.2	-0.1
Aug	-0.1	-0.1	0.2	-0.3
Sep	0.2	-0.1	-0.2	-0.2
Oct	0.2	-0.1	-0.1	-0.6
Nov	-0.3	-0.1	-0.2	0
Dec	-0.2	-0.3	-0.4	-0.3

Appendix C: Grads scripts for displaying COSMO 700hpa winds plots

```
dset ^Oct14.grib
index ^Oct14.grib.idx
undef 9.999E+20
title Oct14.grib
*  produced by grib2ctl v0.9.12.6
dtype grib 255
ydef 497 linear -15.000000 0.062500
xdef 481 linear 23.000000 0.041666
tdef 2 linear 12Z14oct2012 3hr
zdef 1 linear 1 1
vars 2
UGRD700mb  0 33,100,700 ** 700 mb u wind [m/s]
VGRD700mb  0 34,100,700 ** 700 mb v wind [m/s]
ENDVARS


dset ^Oct31.grib
index ^Oct31.grib.idx
undef 9.999E+20
title Oct31.grib
*  produced by grib2ctl v0.9.12.6
dtype grib 255
ydef 497 linear -15.000000 0
xdef 481 linear 23.000000 0.000000
tdef 2 linear 12Z31oct2012 3hr
zdef 1 linear 1 1
vars 2
UGRD700mb  0 33,100,700 ** 700 mb u wind [m/s]
VGRD700mb  0 34,100,700 ** 700 mb v wind [m/s]
ENDVARS


dset ^Nov10.grib
index ^Nov10.grib.idx
undef 9.999E+20
title Nov10.grib
*  produced by grib2ctl v0.9.12.6
dtype grib 255
ydef 497 linear -15.000000 0.062500
xdef 481 linear 23.000000 0.041666
tdef 2 linear 12Z10nov2012 3hr
zdef 1 linear 1 1
vars 2
UGRD700mb  0 33,100,700 ** 700 mb u wind [m/s]
VGRD700mb  0 34,100,700 ** 700 mb v wind [m/s]
ENDVARS
```

```
dset ^Dec26.grib
index ^Dec26.grib.idx
undef 9.999E+20
title Dec26.grib
*  produced by grib2ctl v0.9.12.6
dtype grib 255
ydef 497 linear -15.000000 0.062500
xdef 481 linear 23.000000 0.041666
tdef 2 linear 12Z26dec2012 3hr
zdef 1 linear 1 1
vars 2
UGRD700mb  0 33,100,700 ** 700 mb u wind [m/s]
VGRD700mb  0 34,100,700 ** 700 mb v wind [m/s]
ENDVARS
```